Pergamon

Prog. Energy Combust. Sci. Vol. 21, pp. 1–23, 1995

0360–1285/95 $29.00

0360–1285(94) 00021–2

THEORETICAL ASPECTS OF H/N/O-CHEMISTRY RELEVANT TO THE THERMAL REDUCTION OF NO BY H_2

Eric W. G. Diau,* M. C. Lin,*‡ Y. He and C. F. Melius†

**Department of Chemistry, Emory University, Atlanta, GA 30322, U.S.A.*
†Combustion Research Facility, Sandia National Laboratories, Livermore, CA 94550, U.S.A.

Received 31 October 1994

Abstract—Kinetic modeling of existing data on the reduction of NO by H_2, initiated photolytically or thermally, with a comprehensive reaction mechanism established by means of *ab initio* quantum-chemical and statistical rate-constant calculations, allows us to identify several key elementary processes which are important in different temperature and NO-concentration regimes. At $T < 900$ K, the reduction of NO by H_2 and other hydrides induced photolytically occurs primarily by the bimolecular reaction HNO + HNO → *cis*/*trans*-$(HNO)_2$ under NO-lean conditions, and by the termolecular process HNO + $2NO \rightarrow HN_2O + NO_2$, followed by the fast redox reaction, $HN_2O + NO \rightarrow HN_2 + NO_2$ and N_2 + HONO under NO-rich conditions. In the temperature range of 900 K < T < 1500 K, the reduction of NO by H_2, initiated by the $H_2 + NO \rightarrow H + HNO$ reaction, occurs readily and the global reduction rate is dominated by the $HNO + NO \rightarrow N_2O + OH$ reaction. At temperatures higher than 1500 K, commonly heated by shock waves, the rate of NO reduction is controlled almost exclusively by the $H + NO \rightarrow N + OH$ reaction. The N atom thus formed generates efficiently the O atom by the fast $N + NO \rightarrow N_2 + O$ process. These two NO reduction reactions are greatly enhanced in this temperature regime by the abundance of H atoms, produced by the fast chain processes: $O + H_2 \rightarrow H + OH$ and $OH + H_2 \rightarrow H + H_2O$. The rate constants as well as the mechanisms of these key elementary processes involving H/N/O-species have been interpreted in terms of the theoretical results derived from *ab initio* quantum-chemical and statistical-theory calculations.

CONTENTS

1. INTRODUCTION

The reactions of H/N/O-species are not only important to the combustion of nitramine-based propellants and *N*-containing hydrocarbon fuels, but also relevant to atmospheric chemistry in relation to the formation and reduction of NO_x. The rate constants for many fundamentally significant reactions involving H/N/O-species were surveyed in 1984 by Hanson and Salimian;[1] some of these reactions have recently been updated by Tsang and Herron.[2]

In this article, we focus on the chemistry of H/N/O-species directly connected with the reduction of NO by H_2, taking place thermally or photolytically under well-defined conditions so that kinetic simulation of their chemical transformations can be more readily and reliably performed.

The thermal reaction of NO with H_2 is theoretically quite interesting and challenging, despite its apparent simplicity. To date, the mechanism for the chemical transformation of the H_2–NO system:

$$2NO + 2H_2 \rightarrow N_2 + 2H_2O,$$

has not yet been satisfactorily established, unlike its explosive relative: $H_2 + O_2$, which has attracted far more attention in the history of chemical kinetics

‡Corresponding author.

because of its potential danger as well as its practical importance.

The major difference between these two chemical systems, interestingly, lies only in one electron. In terms of the simple molecular orbital theory, the O_2 and NO molecules have the following molecular electron configurations:

$$O_2[KK(\sigma 2s)^2\ (\sigma^*2s)^2\ (\pi 2p)^4\ (\sigma 2p_z)^2\ (\pi^*2p)^2]$$
$$NO[KK(\sigma 2s)^2\ (\sigma^*2s)^2\ (\pi 2p)^4\ (\sigma 2p_z)^2\ (\pi^*2p)^1].$$

Since NO has one less antibonding electron than O_2, the bond strength of NO is stronger by as much as 32 kcal mol. This added strength in NO effectively prevents the chain reactions analogous to those in the H_2–O_2 system from taking place in the H_2–NO system

$$\begin{aligned} H + NO &\rightarrow NH + O & \Delta H &= +75 \text{ kcal mol} \\ H + NO &\rightarrow N + OH & \Delta H &= +49 \text{ kcal mol}^{-1} \\ O + H_2 &\rightarrow OH + H & \Delta H &= +2 \text{ kcal mol}^{-1} \\ OH + H_2 &\rightarrow H_2O + O & \Delta H &= -14 \text{ kcal mol}^{-1}. \end{aligned}$$

On account of this basic difference and of the experimentally observed approximate third-order kinetics,[3,4] $-d[NO]/dt = k[H_2][NO]^2$, molecular mechanisms were invoked to account for the kinetics and the slowness of the H_2 + NO reaction:[4]

$$\begin{aligned} & 2NO + H_2 \rightarrow N_2 + H_2O_2 \\ & H_2O_2 + H_2 \rightarrow 2H_2O \\ \text{or} \quad & 2NO + H_2 \rightarrow N_2O + H_2O \\ & N_2O + H_2 \rightarrow N_2 + H_2O. \end{aligned}$$

The second stage in either of the alternative mechanisms was assumed to be fast so that the overall kinetics were controlled by the slower third-order processes following the above rate law.

There have been numerous studies on the kinetics and mechanism of the H_2 + NO reaction, since the first investigation by Hinshelwood and co-workers mentioned above, using static cells,[5,6] flow tubes[7,8] and shock tubes.[9–14] It is commonly expected that kinetic data obtained from these methods should be quite different because of the wide variation in both temperature and concentration ranges employed. In pyrolytic studies carried out with static cells and flow tubes, the temperature range below 1500 K usually requires higher reactant concentrations than those used in shock tube experiments ($T > 1500$ K). The reactive species and rate-controlling steps involved under these varying experimental conditions, should be very different. To account for the kinetic data, say, the disappearance rate of NO, $-d[NO]/dt$, measured in different temperature/concentration regimes, a general, unified mechanism to address the expected gradual change in the governing mechanism is required from one regime to another. This task cannot be accomplished without a thorough knowledge of the chemical reactivity and thermochemistry of all major species involved.

For the H_2 + NO reaction, which involves HNO as a major reactive intermediate throughout most of the temperature range studies,[5–14] it appears to be possible for us to establish a comprehensive model to simulate chemical kinetic data obtained from a wide range of experimental conditions. This has been made possible thanks to the recent advances in *ab initio* quantum-chemical calculations for large and complex molecular species, including radicals. For species containing H, N and O atoms, for example, the dimers of HNO, can have a large number of stable geometric isomers. Many of these isomers play their differing roles in the production of HNOH and N_2O in different temperature regimes. The intricate interplays, such as isomerization and decomposition of reactive intermediates, cannot be fully appreciated without reliable thermochemical kinetic data. Most of these data, such as the heats of formation of HNOH and HN(NO)ONO, cannot be obtained experimentally. The latter species is believed to be the intermediate of the newly proposed reaction: $HNO + 2NO \rightarrow HN_2O + NO_2$.[15]

The establishment of this termolecular reaction was aided by a quantum-chemical calculation using the BAC-MP4 (bond-additivity-corrected Møller-Plesset fourth-order perturbation) method[16–18] which will be briefly reviewed in Section 5. The method has been demonstrated to be able to predict the heats of formation of most ground state molecular and radical species containing H/C, H/C/O and H/C/N/O to within ± 2 kcal/mol[17] of those measured experimentally. This is a significant progress indeed. The BAC-MP4 technique has been employed extensively in our recent series of studies to elucidate the kinetics and mechanisms of elementary processes[15,19–26] related to nitramine combustion reactions and the HNCO-RAPRENO$_x$ process,[27] which involves complex and many unknown aspects of a variety of H/N/C/O species.

The mechanism for the thermal reduction of NO by H_2 has been established systematically through detailed computer-modeling of the HNO kinetic data obtained at low temperatures, most importantly the data of Callear and Carr[28] and Cheskis *et al.*[29] The results of the kinetic modeling of these data together with those obtained from the thermal decomposition study of CH_3ONO with and without added NO,[30,31] allow us to construct a unified mechanism for HNO reactions in the presence of varying amounts of NO below 800 K.[15] Under these conditions, the HNO molecule reacts by the following processes:

NO-lean conditions:

$$HNO + HNO \rightarrow \textit{cis/trans}\text{-}(HNO)_2\dagger \xrightarrow{+M} (HNO)_2$$

$$\textit{trans}\text{-}(HNO)_2\dagger \rightarrow HN(OH)NO\dagger \rightarrow HNOH + NO \longrightarrow N_2O + H_2O$$

NO-rich conditions:

$$HNO + 2NO \rightarrow HN(NO)ONO\dagger \rightarrow HN_2O + NO_2,$$

where † represents the vibrational excitation of the denoted species.

Although these processes are adequate in describing the low-temperature reduction of NO, they are insufficient for predicting the rates of NO reduction by H_2 above 900 K obtained from pyrolytic experiments.[3–7] Under these higher temperature, higher reactant concentration conditions, the reaction of NO with HNO,

$$HNO + NO \rightarrow N_2O + OH,$$

first used by Wilde[32] to model the H_2 + NO kinetic data,[5,7] was indeed found to be reasonable and quantum-chemically accountable, as will be discussed later.

At even higher temperatures, accessible conveniently by shock-heating, endothermic processes, such as H + NO → N + OH, become dominant. The bimolecular and termolecular reactions, HNO + HNO and HNO + 2NO, are of negligible relevancy under these conditions due to the low concentration of HNO. The kinetics are hence fully controlled by H, N, O and OH species and, to a minor extent, by NH.

The transition of a dominant reaction mechanism from one regime to another can be most effectively envisaged by the results of sensitivity analyses[33] for reactive species influenced by one or more key processes in different temperature regimes. These analyses revealed that for the thermal reduction of NO by H_2, the following five elementary processes involving H/N/O-species are most important under the indicated conditions:

- 900 K < T < 1500 K (pyrolysis in static cells/flow tubes)
  $H_2 + NO \rightarrow HNO + H$
  $HNO + NO \rightarrow N_2O + OH$
- T > 1500 K (pyrolysis in shock waves)
  $H_2 + NO \rightarrow HNO + H$
  $H + NO \rightarrow N + OH$.

The results of kinetic modeling, aided by the quantum and rate-constant calculations using statistical theories, such as transition state theory (TST),[34] and Rice–Ramsperger–Rice–Marcus (RRKM) theory,[35] for most of the aforementioned reactions will be presented in Sections 2–4, and the comparison of the modeled data for key elementary processes with the predicted values will be made in Section 5.

2. LOW-TEMPERATURE REACTION OF NO WITH H_2 AND OTHER HYDRIDES

Nitric oxide does not react measurably with H_2 at temperatures below 800 K. Most low-temperature studies of NO reactions with H_2 and other hydrides (e.g. HI, CH_2O, CH_3CHO, etc.) were carried out either by direct photolysis or by indirect photosensitization.[36–41] These experiments were designed mostly to study the generation and reaction of HNO.

Recently, we have closely examined many of these low-temperature studies in order to extract kinetic data for the controversial HNO + HNO and HNO + 2NO reactions.[15] We have concluded that the results of two photochemical experiments, both conducted with pulsed irradiation (instead of steady-state photolysis), have been most useful. The experiments are: (1) the flash-photolysis of H_2–NO mixtures carried out over a broad temperature range of 80–420 K by Callear and Carr,[28] and (2) the flash-induced reaction of NO with CH_2O or CH_3CHO at room temperature over a wide NO concentration range by Cheskis *et al.*[29] Computer simulation of these thermally well-defined kinetic data and those obtained by He *et al.*[30,31] from the pyrolysis of CH_3ONO with/without added NO allows us to characterize the kinetics and mechanisms of the above two molecular HNO reactions.[15] The results of these studies are briefly discussed below.

2.1. *HNO Decay Under NO-Lean Conditions*

Callear and Carr[28] studied the thermal reaction of HNO under NO-lean conditions over a broad range of temperature (80–420 K) and pressure (100–750 Torr at 295 K). HNO was generated by the ultraviolet flash photolysis of NO in the presence of an excess amount of H_2. The reaction was believed to be initiated by the reaction of H_2 with electronically excited NO molecules which may be present in several accessible states: $A^2\Sigma^+$, $a^4\Pi$, $B^2\Pi$ and possibly $C^2\Pi$ and $D^2\Sigma^+$ at $\lambda \geq 190$ nm. The HNO production processes, $NO^* + H_2 \rightarrow HNO + H$, $H + NO + M \rightarrow HNO + M$ were much faster than the bimolecular decay process, HNO + HNO → products, so that the decay rates could be readily determined by UV absorption at 207.3 nm employing a deuterium lamp.

The HNO decay rates measured under the NO-lean conditions were found to obey the second-order rate law, provided that the reaction tube employed had been properly conditioned by repetitive flashing of 1-butene. Their data, summarized in a table for the 295 ± 3 K study with information including P_{NO}, P_{total}, $[HNO]_o$, k_{sec} and k_{fst} as well as a graph with k_{sec} obtained for the entire temperature range, allow us to kinetically model the decay rates with our detailed mechanism given in Table 1, using reactions (1)–(33).[15] k_{fst} and k_{sec} mentioned above represent the apparent first-order and second-order rate constants determined by fitting the observed HNO decay rates. The small value of k_{fst}, which was introduced to account for the removal of HNO by a slow first-order process, possibly due to a surface reaction, suggests that the major HNO removal process is the homogeneous second-order associative reaction.

The mechanism proposed for the HNO + HNO association reaction was based on the results of our

Table 1. Unified model for the H_2 + NO system*†

Reaction	*A*	*B*	*E*/R
1. HNO + HNO = ONHNHO (*cis*)	9.3*E*08	0.0	170
2. HNO + HNO = ONHNHO (*trans*)	4.0*E*09	0.0	135
3. HNO + HNO = HNOH + NO	2.0*E*08	0.0	2100
4. HNO + HNO = N_2O + H_2O	9.0*E*08	0.0	1550
5. ONHNHO = HNOHNO	2.4*E*13	0.0	12,300
6. HNOHNO = HNOH + NO	1.0*E*13	0.0	16,000
7. HNOHNO = HONNOH (*t,t,t*)	3.1*E*13	0.0	11,500
8. HONNHO = HN(OH)NO	2.0*E*12	0.0	5750
9. ONHNOH = HONNOH (*t,c,t*)	2.7*E*13	0.0	22,850
10. HONNOH (*t,c,t*) = H_2O + N_2O	4.3*E*11	0.0	8250
11. HNO + NO + NO = HNNO + NO_2	1.7*E*11	0.0	1050
12. HNNO + NO = NNH + NO_2	3.2*E*12	0.0	270
13. HNNO + NO = N_2 + HONO	2.6*E*11	0.0	810
14. HNNO + M = H + N_2O + M	2.2*E*15	0.0	10,800
15. NNH + M = N2 + H + M	1.0*E*14	0.0	1500
16. H_2 + NO = H + HNO	6.29*E*16	−0.89	28,600
17. H + NO + M = HNO + M	5.4*E*15	0.0	−300
18. H + NO_2 = OH + NO	4.9*E*12	0.5	0
19. H + N_2O = OH + N_2	4.4*E*14	0.0	9450
20. OH + H_2 = H_2O + H	1.0*E*08	1.6	1660
21. OH + HNO = H_2O + NO	1.1*E*13	0.0	0
22. NO_2 + H_2 = H + HONO	2.4*E*12	0.0	14,500
23. OH + NO + M = HONO + M	1.6*E*14	−0.5	0
24. HONO + HONO = NO + NO_2 + H_2O	2.3*E*12	0.0	4200
25. HNNO + OH = HNOH + NO	1.0*E*12	0.0	0
26. HNOH + HNO = H_2NOH + NO	1.0*E*12	0.0	1500
27. HNOH + H = H_2 + HNO	1.0*E*12	0.0	0
28. HNOH + OH = H_2O + HNO	1.0*E*12	0.0	0
29. ONHNHO + H = H_2 + NO + HNO	1.0*E*12	0.0	0
30. HNOH + ONHNHO = H_2NOH + HNO + NO	1.0*E*12	0.0	1500
31. OH + HONO = H_2O + NO_2	7.8*E*11	0.0	−380
32. H + H + M = H_2 + M	5.0*E*18	−1.0	0
33. H + OH + M = H_2O + M	1.8*E*22	−1.5	0
34. HNO + NO = OH + N_2O	6.87*E*12	0.0	14,740
35. HONO + M = OH + NO + M	1.8*E*30	−3.9	26,150
36. HNOH + HNO = H_2O + HNNO	1.0*E*12	0.0	0
37. H + HNNO = H_2 + N_2O	1.0*E*13	0.0	0
38. H + HNNO = NH_2 + NO	1.0*E*13	0.0	0
39. H + H_2NOH = H_2O + NH_2	1.0*E*13	0.0	0
40. H + NH_2 + M = NH_3 + M	1.0*E*13	0.0	0
41. NH + HNO = NH_2 + NO	1.0*E*13	0.0	0
42. NH + NO + M = HNNO + M	1.0*E*17	0.0	0
43. NH + H + M = NH_2 + M	1.0*E*18	0.0	0
44. NH + NO = N_2O + H	1.0*E*14	0.0	6400
45. NH + OH = HNO + H	1.0*E*13	0.0	0
46. HNOH + NH_2 = HNO + NH_3	1.0*E*12	0.0	0
47. H + HNOH + M = H_2NOH + M	1.0*E*17	0.0	0
48. NH_2 + OH + M = H_2NOH + M	1.0*E*17	0.0	0
49. NH_2 + NO = N_2 + H_2O	6.2*E*15	−1.25	0
50. NH_2 + NO = N_2 + H + OH	6.4*E*15	−1.25	0
51. HNOH + M = HNO + H + M	1.0*E*16	0.0	27,000
52. H + HNO + M = H_2NO + M	1.0*E*17	0.0	0
53. NH_2 + NO_2 = N_2O + H_2O	1.1*E*12	0.0	0
54. H + NO = N + OH	1.7*E*14	0.0	24,600
55. N + NO = N_2 + O	3.3*E*12	0.3	0
56. H_2 + O = H + OH	1.8*E*10	1.0	4450
57. H_2O + O = OH + OH	6.8*E*13	0.0	9250
58. H + O_2 = OH + O	2.2*E*14	0.0	8450
59. NO + O = N + O_2	3.8*E*09	1.0	20,800
60. NH + O = H + NO	6.3*E*11	0.5	0

* Rate constants are given by $k = AT^B \exp(-E/RT)$ in units of cm^3, mol and s.
† Rate constants for reactions (1)–(33) were taken from Ref. (15). Other rate constants, unless specified otherwise, were taken from Refs (1), (2), (6), (19), (26), (31), (42), (58), (67) and (68).

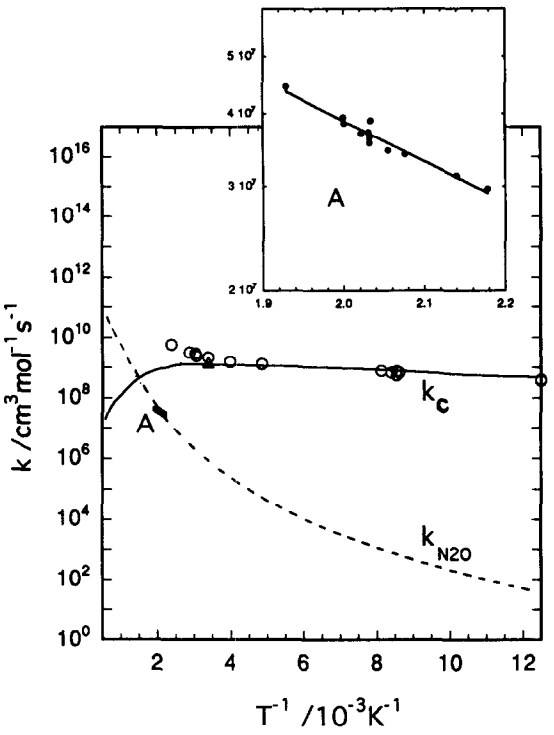

Fig. 1. Temperature dependence of the rate constants for HNO + HNO → H_2O + N_2O (k_{N_2O}) and HNO + HNO → $(HNO)_2$ (k_c). O–Modeled values of Callear and Carr's data from Ref. (28). Δ–Modeled value of Cheskis *et al.*[29] A–Modeled values of He *et al.*[30]

comprehensive quantum-chemical and the associated TST–RRKM calculations for the rate constants of various low-energy reaction paths which are responsible for the decay of the HNO molecule.[15] These theoretical results led us to conclude that, under the conditions employed by Callear and Carr, HNO decayed primarily by the association–stabilization process:

$$HNO + HNO \rightarrow cis/trans\text{-}(HNO)_2\dagger \xrightarrow{+M} cis/trans\text{-}(HNO)_2$$

instead of the formation of the commonly assumed products, N_2O + H_2O. This latter process requires a higher activation energy (3.1 kcal/mol)[30] than that for the association process (0.65 kcal/mol). The association–stabilization process was theoretically found to be pressure-independent above 100 Torr at 295 K, as was reported by Callear and Carr.[28]

The kinetically modeled second-order decay rate constants (denoted as k_c), are presented in Fig. 1 in comparison with the calculated values. Both the absolute values of k_c and its temperature dependence could be satisfactorily accounted for by the theory with the introduction of a small energy barrier for the association reaction, 0.65 kcal mol^{-1}. A least-squares fit to the calculated values for 710 Torr H_2 or He within the 80–420 K temperature range gives $k_c = 10^{16.2}\ T^{-2.40}\ e^{-590/T}\ cm^3\ mol^{-1}\ s^{-1}$ for the association process 2 HNO → $(HNO)_2$.

2.2. *HNO Decay Under NO-Rich Conditions*

The decay of HNO under NO-rich conditions has been studied by Cheskis *et al.*[29] at room temperature using the flash photolysis–laser absorption method with CH_2O or CH_3CHO as the H-source. HNO was generated by the well-known CHO + NO → HNO + CO reaction. NO_2, which could be readily detected by laser absorption, was found to be a major product of the HNO reaction with NO in excess amounts. Since NO_2 and $(HNO)_2$ dimers can be formed in the low-temperature reaction, the result of Cheskis *et al.*, unlike those obtained from the conventional steady-state photolysis method,[36–41] should be free of complications by secondary photolysis of these primary products. Because of this possibility, the data of Holmes and Sundaram[38,39] and Strausz and Gunning[36,37] were not kinetically modeled to extract key reaction rate constants.[15]

The formation of NO_2 was most clearly illustrated by the results of Cheskis *et al.* shown in Fig. 2. Figure 2(a) gives the concentration profiles of HNO and NO_2 measured at the initial conditions: P_{HNO} = 33 mTorr, P_{CH_2O} = 7 Torr and P_{NO} = 230 Torr. Both the HNO decay and the NO_2 formation could be reasonably accounted for by the mechanism given in Table 1. According to this new mechanism, NO_2 derives mainly from the following reactions:[15]

$$HNO + 2NO \rightarrow HN_2O + NO_2 \text{ (slow)}$$
$$HN_2O + NO \rightarrow HN_2 + NO_2 \text{ (fast)}.$$

The theoretical basis of these reactions will be reviewed in Section 5.

Figure 2(b) compares the calculated limiting yield of NO_2 (i.e. $[NO_2]$ at a large reaction time) as a function of added NO over a wide range of its concentration. The observed NO dependence could be well accounted for by the model within the scatter of the experimental data. From the rates of HNO decay in the presence of varying amounts of NO, Cheskis and coworkers also determined the pseudo-first order rate coefficients. The results, summarized in Fig. 3, clearly illustrate the non-linear dependence of these rate coefficients on NO pressure, which can also be quantitatively explained by our new mechanism. It should be pointed out that a stepwise mechanism, similar to that postulated by earlier workers,[36–39] was employed by Cheskis *et al.* to qualitatively account of their NO_2 formation data:

$$HNO + NO \rightarrow HNO{\cdot}NO$$
$$HNO{\cdot}NO + NO \rightarrow NO_2 + N_2 + OH$$

or

$$HNO + NO \rightarrow HO_2 + N_2$$
$$HO_2 + NO \rightarrow NO_2 + OH.$$

These mechanisms, however, are not realistic because the HNO·NO complex is unstable and the formation

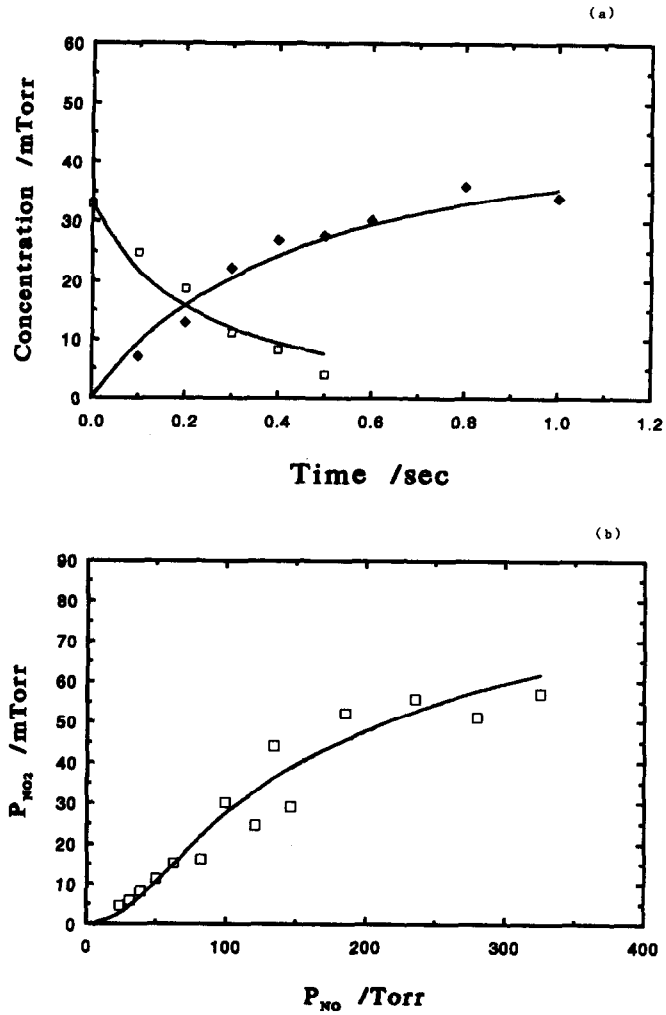

Fig. 2. (a) The concentration profiles of HNO (□) and NO_2 (◆) at initial conditions $P_{HNO} = 33$ mTorr, $P_{CH_2O} = 7$ Torr, and $P_{NO} = 230$ Torr. Solid curves are our modeling results at $T = 298$ K; points are the results of Cheskis *et al.*[29] (b) The concentration profile of NO_2 as a function of NO pressure at $T = 298$ K. Solid curve is our modeling result; points are the results of Cheskis *et al.*[29]

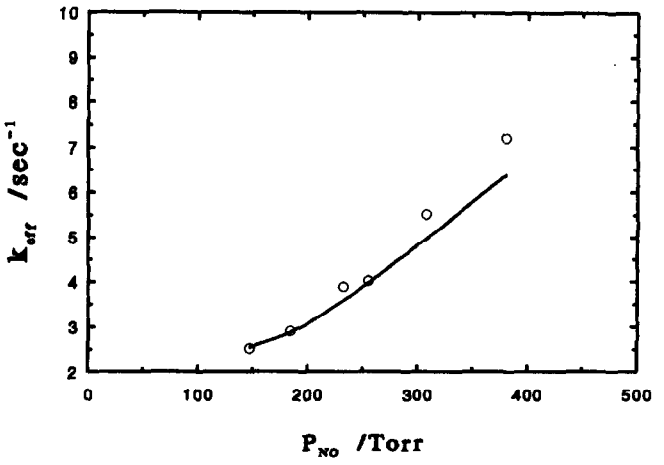

Fig. 3. The first-order coefficient of HNO decay as a function of NO pressure. Data from Cheskis *et al.*[29]

Table 2. Mechanism for the thermal decomposition of CH_3ONO–carbon chemistry*

Reaction	A	B	E/R
1. $CH_3ONO \rightarrow CH_3O + NO$	1.7×10^{15}	0.0	19,480
2. $CH_3ONO \rightarrow CH_2O + NHO$	4.0×10^{13}	0.0	19,380
3. $CH_3O + NO \rightarrow CH_3ONO$	7.2×10^{12}	0.0	0
4. $CH_3O + NO \rightarrow CH_2O + HNO$	8.4×10^{12}	0.0	1030
5. $CH_3O + HNO \rightarrow CH_3OH + NO$	3.2×10^{13}	0.0	0
6. $CH_3O + CH_3O \rightarrow CH_3OH + CH_2O$	7.0×10^{13}	0.0	0
7. $CH_3O + M \rightarrow CH_2O + H + M$	3.9×10^{37}	−6.65	16,760
8. $H + CH_2O \rightarrow CHO + H_2$	2.5×10^{9}	1.27	1330
9. $CH_3O + CH_2O \rightarrow CH_3OH + CHO$	1.0×10^{11}	0.0	1500
10. $CHO + M \rightarrow CO + H + M$	1.9×10^{17}	−1.0	8660
11. $CHO + HNO \rightarrow CH_2O + NO$	2.0×10^{11}	0.7	0
12. $H + CH_3ONO \rightarrow CH_3OH + NO$	1.2×10^{11}	0.0	960
13. $H + CH_3ONO \rightarrow H_2 + CH_2O + NO$	1.4×10^{11}	0.0	960
14. $CHO + NO \rightarrow CO + HNO$	7.2×10^{13}	−0.40	0

*From Ref. (30). This mechanism for the reactions of carbon-containing species together with reactions (1)–(33) given in Table 1 was employed for modeling of the $CH_3ONO + NO$ system.[31] Rate constants, given in terms of $k = AT^B e^{-E/RT}$, have units of cm^3, mol and s.

of HO_2 from the HNO + NO reaction is theoretically implausible. From kinetic modeling of the data presented in Fig. 2(b) and Fig. 3, with a total of 20 data points, the rate constant for the termolecular reaction, $HNO + 2NO \rightarrow HN_2O + NO_2$, has been determined to be $k_{11} = (6 \pm 1) \times 10^9$ cm^6 mol^{-2} s^{-1}.[15] This value compares closely with that of its isoelectronic reaction: $O_2 + 2NO \rightarrow NO_2 + NO_2$, $k = 7.1 \times 10^9$ cm^6 mol^{-2} s^{-1} at 298 K.[42]

2.3. *HNO Reactions in the Thermal Decomposition of CH_3ONO w/wo added NO*

HNO has been suggested by many investigators[43–46] to be a key reactive intermediate in the thermal decomposition of CH_3 ONO responsible for the formation of N_2O by the reaction: $HNO + HNO \rightarrow N_2O + H_2O$.

In a series of recent studies related to the kinetics of CH_3O and HNO reactins,[30,31,47,48] we have carried out detailed product measurements by FTIR (Fourier Transform Infrared) spectrometry over the temperature range of 450–770 K. Products measured included NO, CH_2O, CH_3OH, N_2O and a small amount of CO at higher temperatures. In order to account for the intricate changes in product yields over the range of temperature studied, the effects of pressure and added NO were carefully examined. From this comprehensive set of data, aided by kinetic modeling and RRKM calculations for the unimolecular decomposition of CH_3ONO and the reaction $CH_3O + NO \rightarrow CH_3ONO \rightarrow HNO + CH_2O$, we were able to reliably determine the rate constants for several key processes responsible for the formation of the measured products.[30,31] From the modeling of N_2O formation using the mechanisms given in Tables 1 and 2, we obtained the apparent rate constant for the self-reaction of HNO:

$$HNO + HNO \rightarrow N_2O + H_2O.$$

$k_4 = 10^{8.93 \pm 0.30}$ $e^{-(1550 \pm 150)/T}$ cm^3 mol^{-1} s^{-1} in the temperature range of 450–770 K under NO-lean conditions.[30,31] In this temperature range, the formation and reaction of $(HNO)_2$ dimers, although they were included in the mechanism, did not affect the yield of N_2O noticeably, because of the greater strength of the NH bonds in the dimers.[31]

In the presence of higher concentrations of added NO ($P_{NO} > 50$ Torr), the yield of CH_2O was noted to be reduced due to the production of NO_2 from the $HNO + 2NO \rightarrow HN_2O + NO_2$ and $HN_2O + NO \rightarrow H + N_2 + NO_2$ reactions. The fast $H + NO_2 \rightarrow OH + NO$ reaction effectively sets off the chain processes: $OH + CH_2O \rightarrow H_2O + CHO$, $CHO + M \rightarrow H + CO + M$, and $H + CH_2O \rightarrow H_2 + CHO$, which consume the CH_2O formed in the reaction rather quickly. Thus, from the kinetic modeling of CH_2O yields in the presence of the high concentration of NO, we were able to obtain the rate of the HNO + 2NO reaction for several temperatures between 450 and 520 K. Combination of these data with those derived from the modeling of Cheskis data mentioned above led to the approximate Arrhenius equation, $k_{11} = 10^{11.2 \pm 0.3}$ $e^{-(1050 \pm 200)/T}$ cm^6 mol^{-2} s^{-1}.[31]

Interestingly, the Arrhenius parameters for this termolecular reaction correlate well with those of the analogous reactions previously studied by Christie and coworkers:[49,50] $RNO + 2NO \rightarrow NO_2 +$ products, where R = CH_3, C_2H_5, i-C_3H_7 and n-C_3H_7. The existence of a good linear correlation between $\Delta H^{\ddagger}$ abd $T\Delta S^{\ddagger}$, derived directly from the measured Arrhenius parameters, suggests that the free energies of activation of these reactions are approximately constant and, accordingly, that these reactions may take place via a similar mechanism: $RNO + 2NO \rightarrow RNO(O)NONO \rightarrow R + N_2O + NO_2$.[31]

Table 3. Conditions for the thermal reaction of H_2 with NO used by various investigators

Reference	T/K	P/Torr	Analysis; Reactor
Hinshelwood *et al.*[3,4]	904–1100	< 760	Total pressure change; static cell
Graven[7]	1123–1333	770; 800	H_2O formation by absorption of water in calcium chloride; flow tube
Kaufman and Decker[5]	1173–1425	700	NO decay by UV absorption; static cell
Diau *et al.*[6]	900–1225	700	NO decay and CO_2 formation (when CO is added) by FTIR; static cell

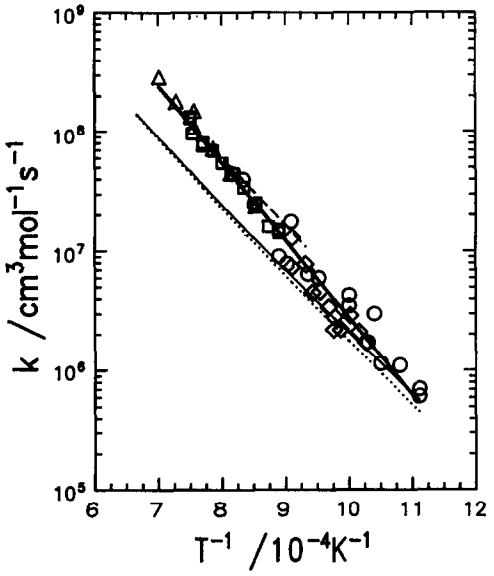

Fig. 4. Arrhenius plots of the rate constant for the reaction HNO + NO → OH + N_2O. Δ, □, ○, and ◇ are kinetically modeled results with the data from Kaufman and Decker,[5] Graven,[7] Diau *et al.*,[6] and Hinshelwood *et al.*,[3,4] respectively. Dashed line: Wilde's modeled result.[32] Solid and dotted lines are the results of RRKM calculations[6] with and without tunneling corrections, respectively, based on PES in G2 level and molecular parameters in QCISD level.[69]

3. THERMAL REDUCTION OF NO BY H_2 BETWEEN 900 AND 1500 K

In the temperature range 900–1500 K, four major studies have been carried out including the pioneering work of Hinshelwood and coworkers,[3,4] with static and flow reactors employing different reaction diagnostic methods which reflected very much the state-of-the-art of their times (see Table 3). This temperature range was effectively limited by the measurability of the chemical change at the low temperature end and the softening of the quartz reaction at the high temperature end.

Hinshelwood and coworkers[3,4] measured the rates of total pressure changes between 900 and 1100 K, covering a broad range of total pressure and the H_2/NO ratio. They also studied the influence of vessel surface by using a smaller quartz bulb containing some powered silica. The result of this test indicated that under the higher pressure conditions (i.e. P_{NO} > 300 and P_{H_2} > 300 Torr), the presence of silica powder did not affect the measured rates. The heterogeneous surface effect became noticeable only at lower pressures.

Graven measured the initial rates of water formation, $\Delta(H_2O)/\Delta t$, gravimetrically at temperatures between 1120 and 1330 K using the flow technique with short reaction times to minimize the chemical conversion to $\leq 5\%$.[7] The total pressure of the system was maintained at 770 or 800 Torr depending on the vessels used. The H_2/NO ratio was varied to examine the overall reaction orders of the reactants.

Kaufman and Decker[5] monitored the rates of NO disappearance continuously by UV photometry. Their results, obtained in the temperature range of 1170–1425 K at a constant total pressure of 700 Torr with He as the diluent, covered a wide range of H_2/NO ratios under the H_2-excess condition.

Recently, in this laboratory, Diau *et al.*[6] studied the H_2 + NO reaction with and without adding CO in the temperature range 900–1225 K near atmospheric pressure conditions using a static cell with FTIR spectrometry. The rates of NO decay and CO_2 formation were determined and utilized for kinetically modeling the rate-controlling HNO + NO reaction. The experimental conditions employed in the four studies are summarized in Table 3 for later reference.

Prior to the present study, there has been one attempt by Wilde[32] to delineate the relative importance of the elementary steps involved in the H_2 + NO reaction in this medium temperature range by computer simulation. The results of the simulation, which focused primarily on the data obtained above 1000 K by Graven[7] and Kaufman and Decker,[5] identified the reaction

$$HNO + NO \rightarrow N_2O + OH$$

with the rate constant, $k_{34} = 10^{12.3\pm0.3}$ $e^{(-13{,}000\pm2500/T)}$ cm^3 mol^{-1} s^{-1}, as an important step in the reduction of NO. The agreement between the observed and calculated overall rates as functions of H_2 and NO was reasonable.

In the present study, all these independent sets of experimental data[3–7] were closely examined and utilized for kinetic modeling with the mechanism presented in Table 1. The goal of our modeling lies not only in the validation of our detailed overall reaction mechanism, but also in the identification and determination of key elementary processes which control the rate of NO reduction in this practical temperature regime.

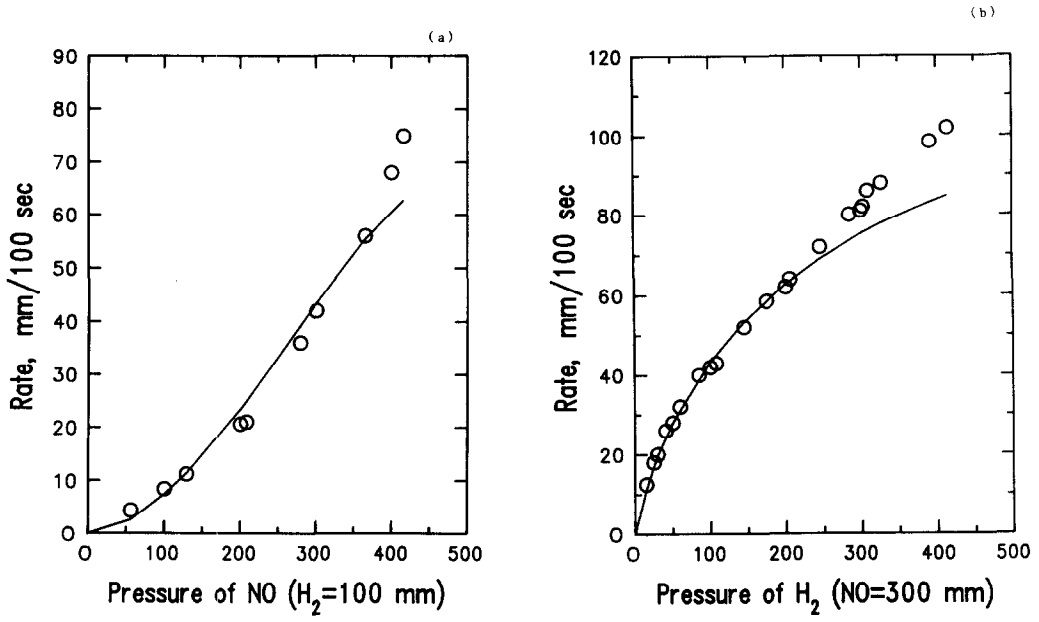

Fig. 5.(a) Comparison between experimental and kinetic-modeling results. The points are experimental reaction rates with respect to NO pressure[4] and solid line is the modeling result[6] at T = 1074 K. (b) Comparison between experimental and kinetic-modeling results. The points are experimental reaction rates with respect to H_2 pressure[4] and solid line is the modeling result[6] at T = 1074 K.

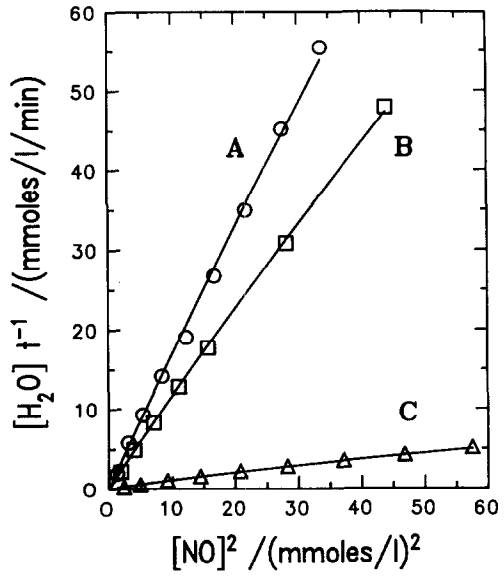

Fig. 6. Comparison of experimental and modeling results. The points are experimental results of Graven[7] for the H_2O formation rate with respect to $[NO]^2$. The experimental conditions: A – T = 1333 K, P = 770 Torr, t = 0.0469 s, $[H_2]$ = 3.49 × 10^{-6} mol cm^{-3}; B – T = 1298 K, P = 800 Torr, t = 0.391 s, $[H_2]$ = 3.31 × 10^{-6} mol cm^{-3}; C – T = 1123 K, P = 800 Torr, t = 0.452 s, $[H_2]$ = 3.79 × 10^{-6} mol cm^{-3}; Solid lines are the modeling results.[6]

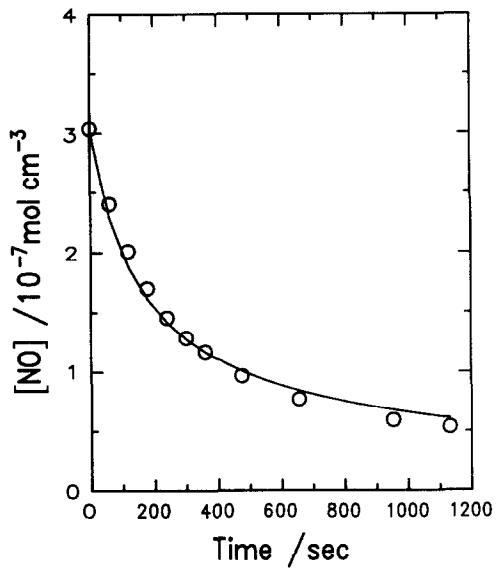

Fig. 7. Comparison of experimental and modeling results. The points denote the experimental results of Kaufman and Decker;[5] the solid curve represents modeled value;[6] the conditions are: P_{H_2} = P_{NO} = 25 Torr, P_{He} = 650 Torr and T = 1323 K.

All of our modeling was performed with the CHEMKIN kinetic program[51] in conjunction with sensitivity analyses,[33] which are indispensable for the identification of key processes affecting the formation and/or destruction of any particular species of interest.

The results of our modeling and sensitivity analyses revealed that in the temperature range 900 K < T < 1500 K, the rate of NO reduction was influenced most pronouncedly by the HNO + NO → N_2O + OH reaction, with a relatively minor contribution from the initiation reaction, H_2 + NO → H + HNO, according to the result of our sensitivity analysis, as was also concluded earlier by Wilde.[32] Therefore, these higher temperature data,

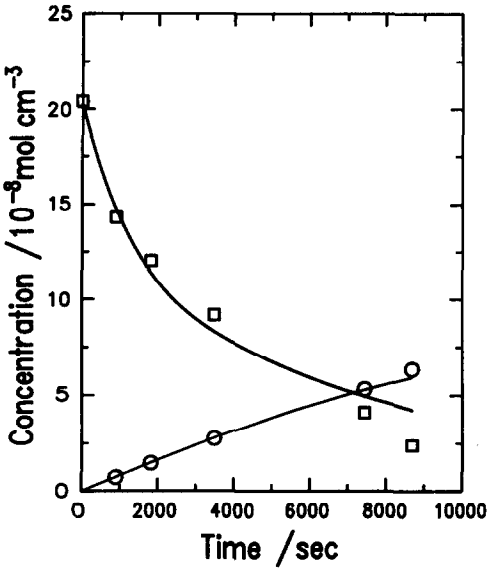

Fig. 8. The concentration profiles of experimental results (□: NO; O: CO_2) and kinetically modeled results (solid curves) for H_2 + NO reaction with CO present.[6] The initial conditions are as follows: T = 1108 K; P = 704 Torr; concentrations for H_2, NO and CO are 3.34, 2.04 and 5.37, respectively, all in units of 10^{-7} mol cm^{-3}.

including our recent results, were fully utilized for the modeling of the HNO + NO reaction. Figure 4 summarizes the modeled results. The least-squares analysis of these results gives rise to

$$k_{34} = 10^{12.84\pm0.06}\, e^{-(14{,}740\pm180/T)}\ \text{cm}^3\ \text{mol}^{-1}\ \text{s}^{-1},$$

where the uncertainties represent one standard deviation. With Hinshelwood's data, derived exclusively from total-pressure measurements, we modeled the rates of the overall pressure change given by these authors[3,4] by varying the value of k_{34} to give the best fits (see Ref. (6) for details). These results, however, are expected to be less reliable than those obtained from the modeling of kinetic data by Graven,[7] Kaufman and Decker,[5] and Diau *et al.*[6]

In Figs 5–8, we compare the calculated values for the total rates of the H_2 + NO reaction obtained by Hinshelwood and coworkers[4] as functions of H_2 and NO concentrations, for the rates of H_2O production by Graven[7] at three different temperatures, for the rate of NO decay by Kaufman and Decker[5] at 1323 K, and for the rates of NO decay and CO_2 formation by Diau *et al.*[6] at 1108 K. The modeling was performed with the mechanism given in Table 1 using the average rate constants for the major proc-

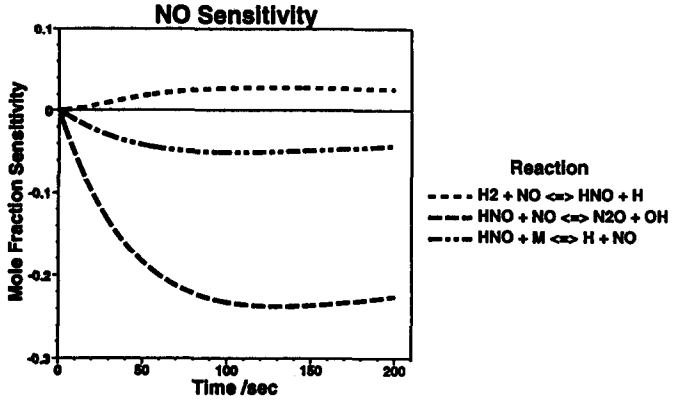

Fig. 9. Normalized sensitivity coefficients for NO corresponding to Hinshelwood's experimental conditions:[4] P_{H_2} = 600 Torr, P_{NO} = 100 Torr and T = 1098 K.

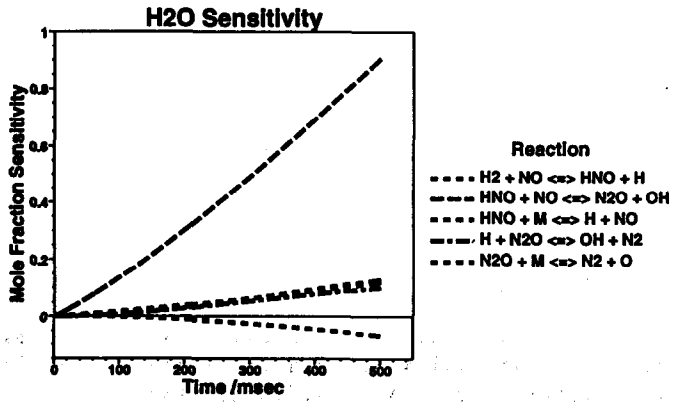

Fig. 10. Normalized sensitivity coefficients for H_2O corresponding to Graven's experimental conditions:[7] $[H_2]$ = 2.01 × 10^{-6} mol cm^{-3}, [NO] = 3.31 × 10^{-6} mol cm^{-3}, P = 800 Torr and T = 1298 K.

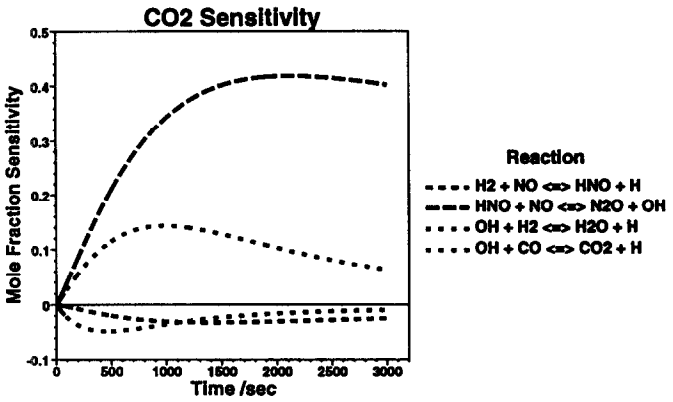

Fig. 11. Normalized sensitivity coefficients for CO_2 corresponding to Diau *et al.*'s experimental conditions:[6] $[H_2] = 2.6 \times 10^{-7}$ mol cm^{-3}; $[NO] = 1.6 \times 10^{-7}$ mol cm^{-3}, $[CO] = 3.9 \times 10^{-7}$ mol cm^{-3}; $P =$ 706 Torr; $T = 1200$ K.

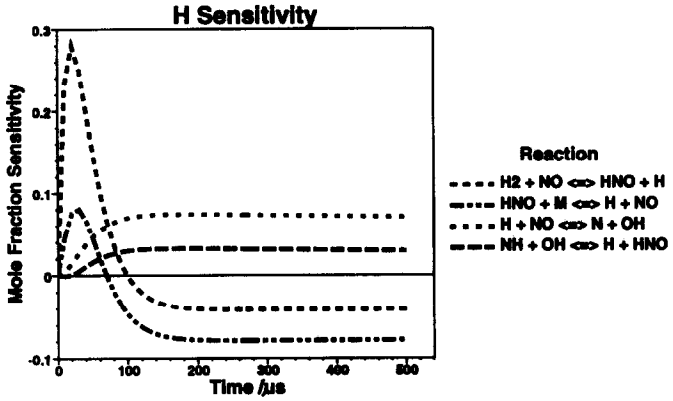

Fig. 12. Normalized sensitivity coefficients for the H atom corresponding to Natarajan and Roth's experimental conditions:[52] $T = 2050$ K, $[H_2] = 3.04 \times 10^{-8}$ mol cm^{-3}, $[NO] = 6.08 \times 10^{-8}$ mol cm^{-3} and $[Ar] = 5.95 \times 10^{-6}$ mol cm^{-3}.

esses derived above. The agreement between the calculated and experimentally measured values using totally different methods appears to be quite satisfactory.

Figures 9–11 show the results of sensitivity analyses which demonstrate the effects of these and other processes on the decay of NO and the production of H_2O as well as CO_2 under different conditions employed in the individual studies.

4. THERMAL REDUCTION OF NO BY H_2 ABOVE 1500 K

There have been numerous studies of the H_2 + NO reaction above 1500 K[8–14,42] primarily with the shock tube, the best tool available today for homogeneous, instantaneous heating to very high temperatures. In a flow study by Hanson and coworkers,[8] a high-temperature ceramic tube was employed. Most recent studies, except the unpublished work of Natarajan and Roth,[52] have been summarized by Hanson and Salimian[1] in conjunction with the H + NO → N + OH reaction.

In the study by Natarajan and Roth,[52] the concentration of H atoms formed in the H_2 + NO reaction between 1800 and 2300 K was monitored by the resonance absorption with the Lyman-α (121.16 nm) line. Since the H-atom concentration depends quite sensitively on the initiation reaction, H_2 + NO → HNO + H, as shown in Fig. 12, they have successfully determined its rate constant by kinetic modeling:

$$k_{16} = 8.5 \times 10^{13}\, e^{(-27,500/T)}\ \text{cm}^3\ \text{mol}^{-1}\ \text{s}^{-1}.$$

This result is presented graphically in Fig. 13(a) together with the values determined from other studies[13,53] as discussed earlier. Asaba and coworkers[9,13] reported the rate constant $k_{16} = 10^{13.5 \pm 0.5}\, e^{(-27,800/T)}$ cm^3 mol^{-1} s^{-1}, which is close to the result of Natarajan and Roth[52] as well as the values calculated from the theoretical result of Soto and Page[53] for the H + HNO reaction.

Most interestingly, the theoretical result of Soto and Page[53] for the reverse reaction H + HNO → H_2 + NO, transformed into that for the

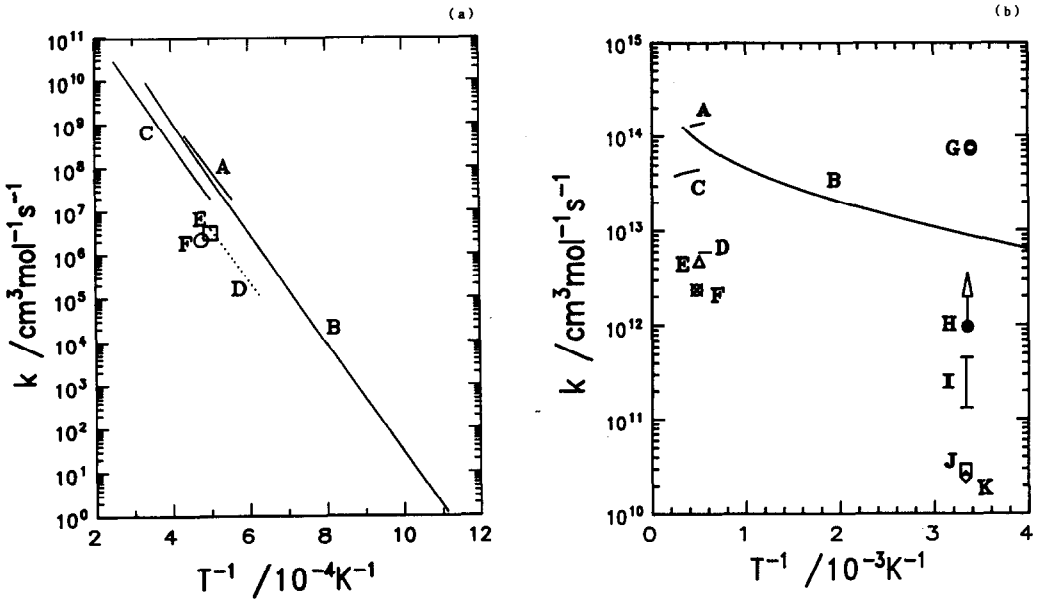

Fig. 13. Temperature dependence of the rate constants for the reaction, $H_2 + NO \rightarrow H + HNO$ (a), and its reverse reaction, $H + HNO \rightarrow H_2 + NO$ (b). References: A—Natarajan and Roth;[52] B—Soto and Page;[53] C—Ando and Asaba;[13] D—Bulewicz and Sugden;[65] E—Halstead and Jenkins;[66] F—Smith;[59] G—Dodonov *et al*;[60,61] H—Washida *et al.*;[62] I—Kohout and Lampe;[41] J—Clyne and Thrush;[63] K—Lambert.[64]

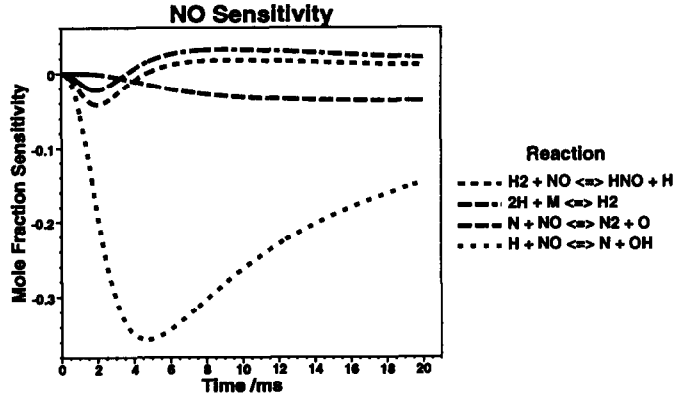

Fig. 14. Normalized sensitivity coefficients for NO corresponding to Asaba's experimental conditions:[12] $T = 2400$ K, $[H_2] = [NO] = 6.01 \times 10^{-8}$ mol cm^{-3} and $[Ar] = 5.89 \times 10^{-6}$ mol cm^{-3}. The NO reduction rate is seen to be insensitive to the $H_2 + NO$ reaction.

forward process with the equilibrium constant evaluated from the JANAF thermochemical data,[54] agrees quite well with these high temperature results. In Fig. 13(b), we compare Soto and Page's theoretical rate constant for H + HNO with experimental values over a broad range of conditions. The poor quality of the experimental work is obvious. However, for kinetic simulation, we strongly recommend the use of Soto and Page's result. The mechanism for the $H_2 + NO$ reaction will be discussed in the following section.

Because most of the high temperature experiments, except that of the Roth group,[52] monitored the removal rates of NO, which depend most strongly on the rate of $H + NO \rightarrow N + OH$ reaction, the measured kinetic data were utilized to evaluate the rate constant for this rate-controlling step. The dominant effect of the H + NO reaction on the concentration of NO is clearly illustrated in Fig. 14 by the result of a sensitivity analysis performed for $T = 2400$ K and $P = 1.16$ atm.

The values of the rate constant for the $H + NO \rightarrow N + OH$ reaction evaluated by various workers are summarized in Fig. 15(a). Hanson and Salimian[1] have critically reviewed these data and recommended the following expression:

$$k_{54} = 1.7 \times 10^{14} e^{(-24,600/T)} \text{ cm}^3 \text{ mol}^{-1} \text{ s}^{-1}$$

for the temperature range 1800–4200 K. The recommended value is quite reliable and consistent with the

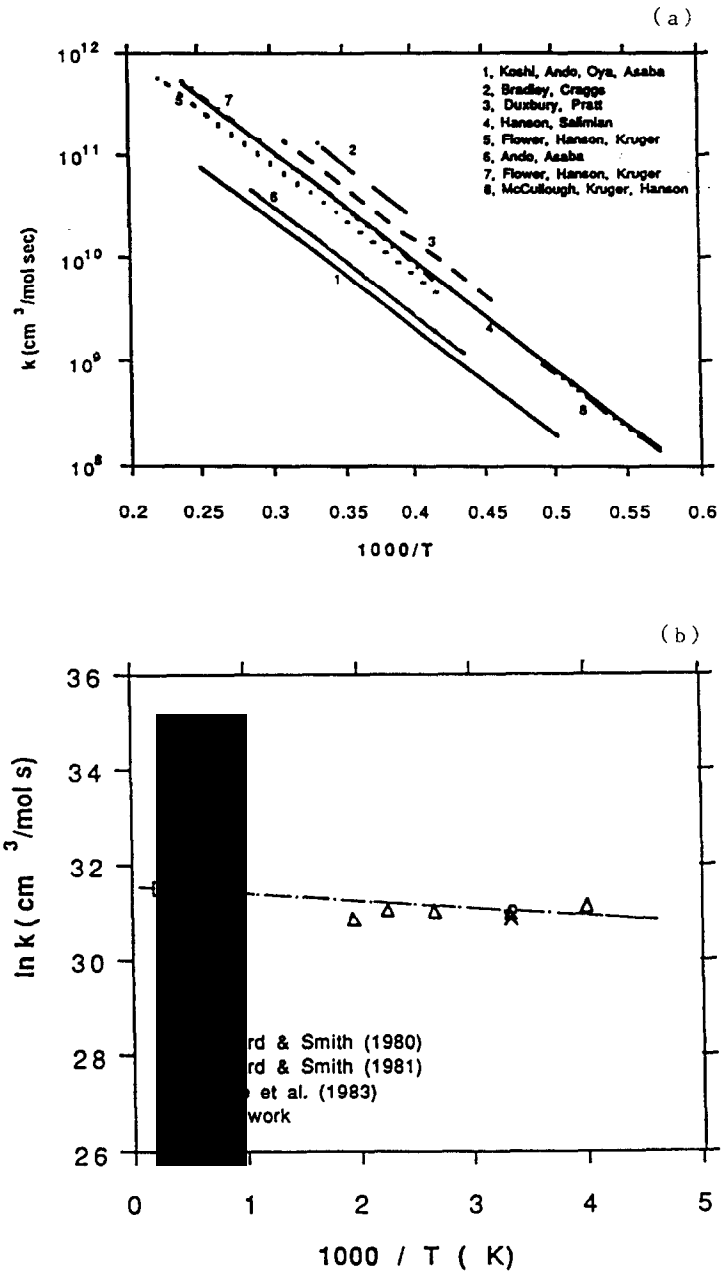

Fig. 15. Temperature dependence of the rate constant for the reaction, H + NO → OH + N (a), and its reverse reaction, OH + N → H + NO (b). References: (a): 1—Koshi *et al.*,[9] 2—Bradley and Craggs;[11] 3—Duxbury and Pratt;[12] 4—Hanson and Salimian;[1] 5—Flower *et al.*;[10] 6—Ando and Asaba;[13] 7—Flower *et al.*;[14] 8—McCullough *et al.*;[8] (b): O—Howard and Smith;[55] Δ—Howard and Smith;[56] X—Brune *et al.*[57]

rate constant for the reverse reaction measured at low temperatures summarized in Fig. 15(b). Further discussion on the mechanism of the H + NO = N + OH reaction will be presented in the following section.

5. THEORETICAL INTERPRETATION OF KEY ELEMENTARY PROCESSES

The kinetic modeling of NO reduction by H_2, including that induced by photoexcitation at low temperatures, with the mechanism given in Table 1 has identified the following five reactions to be pivotal in different temperature regimes:

- $T < 900$ K
  $HNO + HNO \rightarrow (HNO)_2$
  $HNO + 2NO \rightarrow HN_2O + NO_2$
- 900 K $< T <$ 1500 K
  $HNO + NO \rightarrow N_2O + OH$
- $T >$ 1500 K

Table 4. Energetics of key species involved in the present system calculated by the BAC-MP4 method*

Species	$\Delta H^{\circ}_{f,0}$/kcal mol^{-1} JANAF	BAC-MP4
H	51.67	51.62
NO	21.48	21.56
OH	9.17	9.50
HNO	24.52	24.09
HNN	—	60.39
N_2O	20.44	19.39
NO_3	7.73	7.83
H_2O	−57.16	−57.78
HNOH (*cis*)	—	28.90
HNOH (*trans*)	—	22.72
HONO (*cis*)	−16.87	−16.13
HONO (*trans*)	−17.37	−17.50
HNNO (*cis*)	—	56.69
HNNO (*trans*)	—	59.76
HNOH	—	−9.66
ONHNHO (ONNO *cis*)	—	30.98
ONHNHO (ONNO *trans*)	—	26.79
HN(OH)NO(ONNO *trans*)	—	18.04
ONHNOH (ONNO *cis*, HONN *trans*)	—	6.57
HON=NOH (*cis, trans, trans*)	—	5.74
HN(NO)ONO	—	58.37
-NONH(O)ON-(cyclic)	—	81.15
HNNONO (*cis, trans, trans*)	—	61.51
HNNONO (*trans, trans, trans*)	—	62.72
$HN(NO)_2$(NNNO *cis, trans*)	—	59.92
$HN(NO)_2$(NNNO *trans, trans*)	—	52.73
HN(O)NO	—	47.01

* Data from Ref. (15).

$$H_2 + NO \rightarrow HNO + H$$
$$H + NO \rightarrow N + OH.$$

The comprehensive mechanism was established with the aid of quantum-chemical and statistical-mechanical rate constant calculations as alluded to earlier. The theoretical bases of these reactions, particularly for the complex systems such as HNO + HNO and HNO + 2NO reactions, are indispensable for us to unravel the unknown mechanisms involved.

The fundamental mechanisms (i.e. the detailed reaction paths and the transition states) of the above five reactions have recently been studied by *ab initio* quantum calculations with the BAC-MP4 method developed by Melius and coworkers.[16-18] The energetics of various species relevant to the H/N/O-chemistry computed by this technique are summarized in Table 4. For the H + HNO → H_2 + NO reaction, Soto and Page[53] have performed a more extensive *ab initio* quantum-chemical study in conjunction with a canonical variational transition state reaction-rate calculation for the direct abstraction process. The results of these theoretical calculations are summarized below for the individual reactions.

5.1. *The BAC-MP4 Theoretical Method*

The determination of reaction mechanisms requires knowledge of the thermochemistry (i.e. enthalpies, entropies and free energies) of all the possible species involved in the reaction. This includes not only the reactants and products, but also intermediates as well as transition state structures connecting these species. The determination of the thermochemical properties requires knowning the molecular geometries, vibrational frequencies, and bond dissociation energies (BDEs). The BAC-MP4 method has been developed to generate reliable theoretical results. This has been particularly important for species involving nitrogen-containing species. Nitrogen can change its chemical bonding characteristics during reactions from trivalent as in HNO to hypervalent to dative bonded as in N_2O. Thus, it has been necessary to develop a method which did not assume a priori knowledge of the chemical bond. As mentioned in previous sections, many of the intermediates and transition state structures involved in the H/N/O chemistry were not previously known.

The details of the BAC-MP4 theoretical approach have been described in detail elsewhere.[16-18] In this section we present a summary of the method. Molecular geometries are determined for each stationary point on the potential energy surface (PES) of the reaction system. Stable structures correspond to minima on the PES, i.e. structures which have zero imaginary frequencies, while transition state structures correspond to structures which have one imaginary vibrational frequency. The geometries were optimized using the Hartree–Fock method (restricted Hartree–Fock, RHF, for closed shell species and unrestricted Hartree–Fock, UHF, for open shell species). A split-valence with polarization functions on the heavy atoms (6–31G*) basis set was used to describe the electronic wave function. Harmonic vibrational frequencies for each of the structures were then calculated at the same level of theory (RHF or UHF) with the same basis set (6–31G*). Since the vibrational frequencies at this level of theory tend to be too large compared to experimental values, the HF harmonic frequencies were scaled downward by 12%. To determine atomization enthalpies (which lead to BDEs) electron correlation effects were included by performing MP4 order perturbation theory calculations including single, double, triple, and quadruple excitations. The 6–31G** basis set was used for the MP4 calculations.

The resulting bond dissociation energies still contain systematic errors e.g. the BDEs are too small, with the error increasing with the shortening of the bond length. BACs have been derived to correct these systematic errors. The BAC procedure has been described in detail elsewhere.[17,18] For a chemical bond between atoms X_i and X_j in the molecule $X_k - X_i - X_j$ the BAC has the form $BAC(X_j - X_j) = f_j g_{kij}$, where $f_{ij} = A_{ij} \exp(-\alpha_{ij} R_{ij})$, $g_{kj} = (1 - h_{ik} h_{ij})$, and $h_{ik} = B_k \exp[-\alpha_{ik}(R_{ik} - 1.4\text{Å})]$. A_{ij} and α_{ij} depend on the bond type X_i and X_j. For the H/N/O system, $A_{NN} = 472.62$, $\alpha_{NN} =$

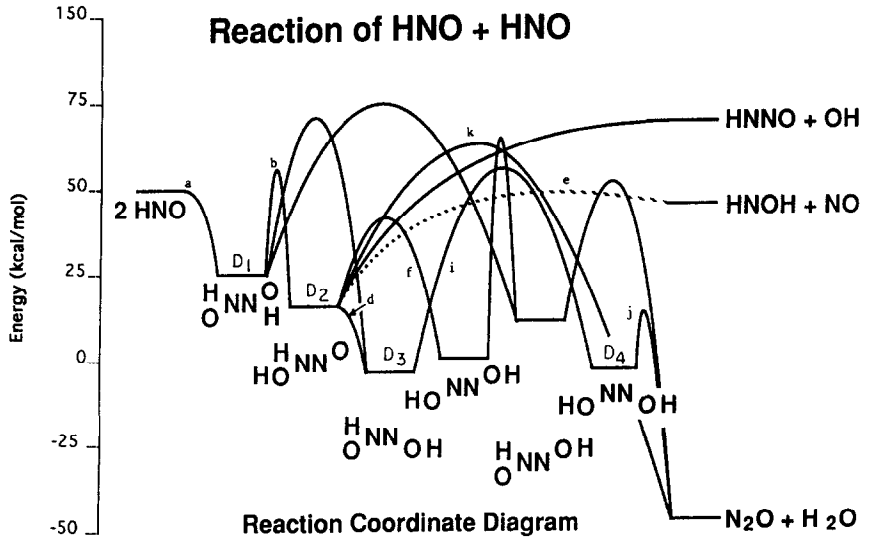

Fig. 16. The energy diagram for the HNO + HNO reaction based on the result of BAC-MP4 calculations.[15]

2.6, A_{NO} = 226.04, α_{NO} = 2.1, A_{NH} = 70.08, α_{NH} = 2.0, A_{OH} = 72.45, α_{OH} = 2.0, while β_H = 0.0, β_N = 0.2 and β_O = 0.225. There are additional corrections for spin contamination as discussed elsewhere.[16,17] Examples of heats of formation for nitrogen-containing species using the BAC-MP4 method are given in Table 4. Additional heats of formation of nitrogen-containing species can be found in Ref. (16).

5.2. *HNO + HNO → products*

The bimolecular self-reaction of HNO is far more complex than had been assumed previously.[15] The result of our recent comprehensive quantum calculation with the BAC-MP4 method has revealed the presence of numerous geometric isomers with comparable thermal stabilities. The formation of most of these isomers are, however, kinetically limited in the HNO + HNO reaction.[15] Those isomers which are relevant to the production of $N_2O + H_2O$ and HNOH + NO are presented in the reaction coordinate diagram in Fig. 16. The reactions which may occur along the lowest energy paths leading to these and dimeric products by collisional stabilization are schematically presented below: where D_1 = *trans*-$(HNO)_2$, D_2 = HN(OH)NO, D_3 = HN(O)NOH and D_4 = *cis*-HNNOH (Scheme 1).

According to the above raction scheme and the energy diagram presented in Fig. 16, the rates of HNO decay measured at low temperatures (T < 420 K) were controlled entirely by the recombination reaction producing *cis*- and *trans*-$(HNO)_2$ which can be calculated by Eq. (15):

$$k_c = \frac{kT}{h}\frac{Q_{vr}^{\ddagger}}{Q^2_{HNO}} e^{-E_a/RT} \int_0^{\infty} \frac{\omega \Sigma \rho(E^{\ddagger}) e^{-E^{\ddagger}/RT}}{k_{-a}(E) + k_b(E) + \omega} d\left(\frac{E^{\ddagger}}{RT}\right) \quad (1)$$

The production of $N_2O + H_2O$ and HNOH + NO decomposition products, which occurs at higher temperatures following the isomerization process (b), requires higher activation energy. The rate constants for the fragmentation and isomerization of the excited D_2[HN(OH)NO] isomer can be computed in principle by Eq. (15):

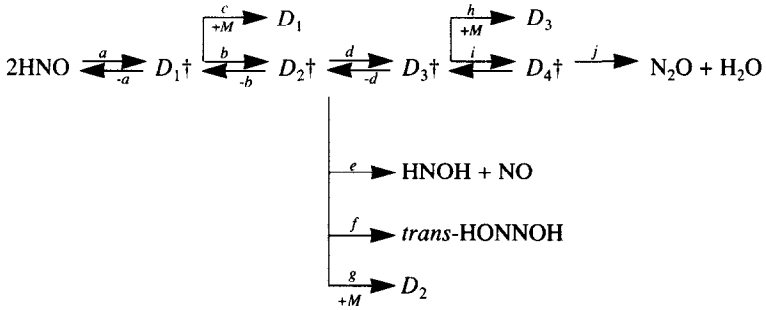

Scheme 1.

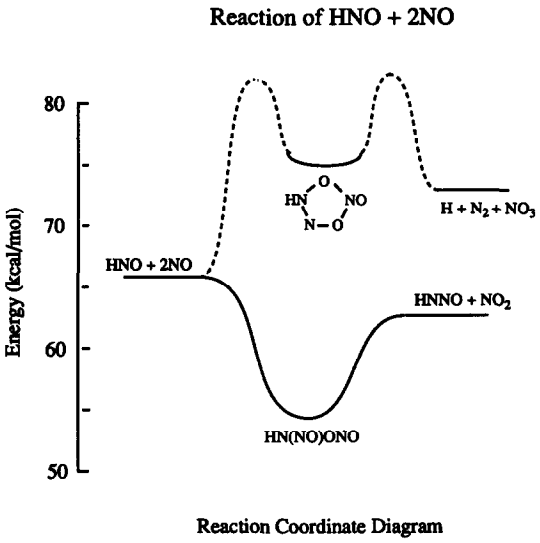

Fig. 17. The energy diagram for the HNO + 2NO reaction based on the result of BAC-MP4 calculations.[15]

$$k_{D_n} = \frac{kT}{h}\frac{Q_{tr}^{\ddagger}}{Q^2_{HNO}} e^{-E_n/RT} \int_{\Delta E_{ab}}^{\infty} \frac{k_b(E)\Sigma p(E^{\ddagger})\alpha_{D_n}(E)}{k_{-a}(E) + k_b(E) + \omega} d\left(\frac{E^{\ddagger}}{RT}\right) \quad (2)$$

where $\alpha_{D_n}(E)$ is the branching ratio for the formation of the D_n isomer and the decomposition products such as HNOH + NO, etc. ΔE_{ab} is the energy barrier difference at a and b as labeled in Fig. 16. The definitions of other symbols associated with TST–RRKM formulations for complex-forming bimolecular processes can be found in Ref. (15).

For the formation of $N_2O + H_2O$, which is controlled by the isomerization step producing the D_3 isomers, HN(O)NOH, rather than by the elimination of H_2O in the final step on account of the very low reaction barrier E_j (see Fig. 16), $\alpha_{N_2O} = k_d k_l/(k_{-d} + k_i + w)B$; where $B = k_{-b} + k_d + k_e + k_j + \omega - A$, with $A = k_d k_{-d}/(k_{-d} + k_i + \omega)$.[15] Here all the specific rate constants are functions of internal energies as indicated in Eqs. (1) and (2). The production of N_2O is competitive with the formation of HNOH + NO, whose effect on N_2O formation is still unclear. In addition, the effect of quantum-mechanical tunneling on H-migration reactions may be important at low temperatures. These effects, together with that of the collisional deactivation of the excited dimers requires further careful calculations.

The rate constant for the dimerization of HNO computed with Eq. (1), using the transition state parameters predicted by the BAC-MP4 method[15] is presented in Fig. 1. The theoretical results satisfactorily reconcile the fast rates of HNO decay measured by Callear and Carr[28] and the slow rates of N_2O formation reported by He *et al.*[30,31]

The rate constants of other reactions given in Table 1 derived from the stabilized products of the HNO + HNO reaction were all calculated by the TST or the RRKM theory for 710 Torr of He or H_2. Above 420 K, the reactions of the stabilized $(HNO)_2$ and its isomers are unimportant.[31] They decay primarily by thermal decomposition reactions as indicated in the overall reaction mechanism (Table 1). It should be mentioned that the presence of HNOH has minor kinetic consequence because of its high stability. At higher temperatures ($T > 900$ K), it decomposes to give back HNO with no noticeable effect on the rapid $H_2 + NO = H + HNO$ equilibrium.

5.3. *Reactions of HNO with NO*

As discussed in the preceding section, HNO undergoes bimolecular and termolecular reactions with NO, depending on the concentration of NO and the temperature of the system. Under low-temperature and NO-rich conditions, the termolecular process takes place readily with small activation energy via a short-lived intermediate:

$$HNO + 2NO \rightarrow HN(NO)ONO \rightarrow HN_2O + NO_2.$$

This reaction is analogous to its isoelectric reaction, $O_2 + 2NO \rightarrow O(NO)ONO \rightarrow 2NO_2$ which occurs with a small negative activation energy.[42] The energy diagram for the termolecular reaction is shown in Fig. 17. As indicated in the diagram, the formation of $HN_2O + NO_2$, akin to the production of $NO_2 + NO_2$ from the $2NO + O_2$ reaction, is exothermic and has a negligible reaction barrier; therefore, it can occur readily at low temperatures. On the other hand, the previously assumed mechanism taking place by a five-centred intermediate requires a rather high activation energy ($E_a > 14$ kcal/mol, see Fig. 17), which would prevent it from occurring at room temperature, contrary to experimental findings.

At higher temperatures under the conditions employed in the studies of the $H_2 + NO$ reaction ($900 \text{ K} < T < 1500$ K), the reaction of HNO with NO is dominated by its bimolecular process, which occurs by the rate-limiting H-migration step (b):

$$HNO + NO \rightleftharpoons HN(NO)O \xrightarrow{b} HONNO \xrightarrow{c} HO + N_2O.$$

A simplified energy diagram constructed according to the result of a BAC-MP4 calculation listed in Table 5 is presented in Fig. 18. The barrier for H-migration process is calculated to be 25 kcal mol^{-1} above HNO + NO (or approximately HN(NO)O which is unstable), close to a theoretical value of 23 kcal mol^{-1} obtained with higher levels of theory by Mebel *et al.*[69] and the activation energy measured experimentally, 29 kcal mol^{-1}. The calculated rate constant based on the predicted TS parameters, shown in Fig. 4, is compared with the modeled values, including the ones by Wilde.[32] Since the NO

Table 5. Molecular parameters for the HNO + NO → N_2O + OH reaction*

Species	$\Delta H^\circ_{f,o}$/kcal mol^{-1}	I_A, I_B, I_C/amu	ν_i/cm^{-1}	
HN(O)NO (^{2}A″)		25.513	247.4	427.7
ONNO *trans*	45.69	327.982	588.9	665.3
		353.495	1104.0	1280.5
			1358.5	1514.3
			3326.9	
HN(O)NO (^{2}A″)		67.539	299.9	364.9
ONNO *cis*	47.01	234.499	530.7	886.9
		302.036	979.2	1195.8
			1372.8	1507.2
			3412.7	
HN(O)NO (^{2}A′)		73.831	308.3	402.3
ONNO *cis*	74.96	225.840	625.6	797.6
		229.652	939.7	1088.9
			1435.0	1574.2
			3385.6	
HN(O)NO (^{2}A′)		26.892	211.9	382.5
ONNO *trans*	83.21	338.276	529.7	616.4
		365.169	1000.5	1040.0
HONNO (^{2}A′)		21.565	334.8	337.8
ONNO *trans*,	51.17	344.908	368.9	621.8
HONN *trans*		365.664	998.1	1115.0
			1161.7	1432.7
			3670.0	
HONNO (^{2}A′)		23.449	342.2	359.9
ONNO *trans*,	53.84	340.468	433.7	629.8
HONN *cis*		363.917	1016.2	1094.1
			1173.8	1428.3
			3560.8	
HONNO (^{2}A′)		73.618	172.6	298.3
ONNO *trans*,	49.94	223.960	521.6	654.3
HONN *cis*		297.579	968.5	994.6
			1231.2	1417.2
			3593.1	
HONNO (^{2}A′)		74.824	313.9	391.0
ONNO *cis*,	48.09	216.128	545.1	748.3
HONN *trans*		290.951	973.9	1013.4
			1226.0	1419.4
			3667.0	
HONNO (^{2}A″)		24.390	260.1	435.8
ONNO *trans*,	53.91	334.869	468.8	661.0
HONN *trans*		369.257	958.4	1171.2
			1216.9	1446.5
			3656.0	
HONNO (^{2}A″)		25.954	271.1	431.9
ONNO *trans*,	53.07	330.235	545.1	665.4
HONN *cis*		356.189	976.5	1183.3
			1254.8	1437.5
			3529.5	
HONNO (^{2}A″)		76.864	363.0	448.2
ONNO *cis*,	52.21	212.314	524.8	834.0
HONN *cis*		289.718	891.3	1052.7
			1216.8	1420.7
			3538.8	
HONNO (^{2}A″)		74.546	222.9	399.0
ONNO *cis*,	55.88	218.985	482.5	810.8
HONN *trans*		293.530	918.8	1052.7
			1237.7	1418.1
			3654.8	

* The data given for a chemical reaction represent those of its transition state.

Table 5. *Continued*

Species	$\Delta H^{\circ}_{f,o}$/kcal mol^{-1}	I_A, I_B, I_C/amu	ν_i/cm^{-1}	
HN(O)NO→		27.439	−2545.6	
HONNO (^{2}A″)	70.63	305.029	300.2	799.4
		332.468	519.0	1145.5
			1277.8	1333.9
			1375.6	2023.5
HN(O)NO→		26.064	−2262.7	
HONNO (^{2}A′)	105.45	327.900	210.8	403.9
		347.964	743.9	1024.9
			1115.1	1193.8
			1261.3	2060.5
N_2O + OH→		76.099	−819.2	
HONNO (^{2}A′)	47.39	266.352	54.7	238.5
ONNO *cis*,		342.451	486.0	636.3
HONN *cis*			1061.0	1190.6
			1597.8	3578.4
N_2O + OH→		75.983	−791.6	
HONNO (^{2}A′)	43.90	264.134	209.9	219.4
ONNO *cis*,		340.117	490.6	590.6
HONN *trans*			1033.2	1194.0
			1621.0	3621.8
N_2O + OH→		29.203	−725.6	
HONNO (^{2}A′)	50.36	383.814	197.8	264.5
ONNO *trans*,		413.017	336.0	541.0
HONN *trans*			1008.9	1183.5
			1593.5	3625.9

* The data given for a chemical reaction represent those of its transition state.

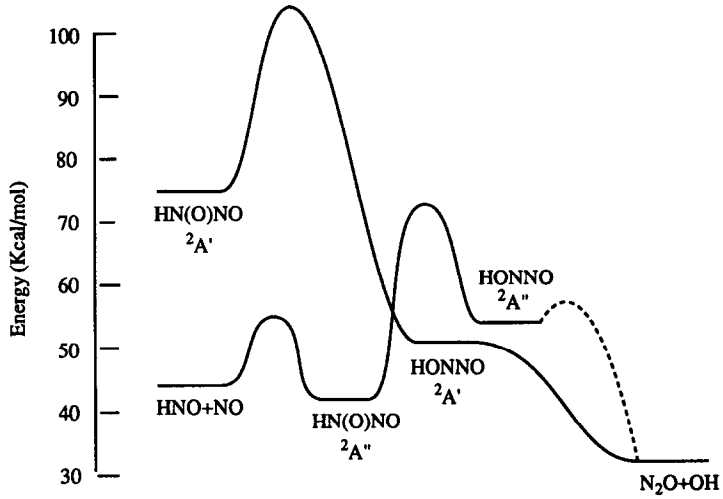

Fig. 18. The energy diagram for the HNO + NO → N_2O + OH reaction based on the result of BAC-MP4 calculations (this work).

reduction rate in this temperature regime is strongly affected by the HNO + NO reaction, according to the result of the sensitivity analysis given in Fig. 9, Wilde's values based on a much simpler mechanism agree closely with ours.

5.4. *The H_2 + NO = H + HNO Reaction*

The H_2 + NO reaction is the key initiation reaction in the thermal reduction of NO by H_2 below 4000 K. At higher temperatures, the dissociation of H_2: H_2 + M = 2H + M becomes competitive. For a 1% NO mixture at atmospheric pressure, the two competitive initiation processes contribute equally at about 3750 K. The reverse H + HNO process is, however, relevant to the low-temperature reaction of HNO. It becomes less important above 1500 K because of the low concentration of HNO, resulting

Table 6. Molecular parameters for the $H_2 + NO \rightarrow H + HNO$ reaction computed by the BAC-MP4 method

Species	$\Delta H^\circ_{f,o}$/kcal mol^{-1}	I_A, I_B, I_C/amu	ν_i/cm^{-1}	
H_2NO ($^2A'$)		5.728	608.1	1277.8
	17.48	52.353	1288.1	1641.6
		57.004	3325.1	3450.2
HNOH ($^2A''$)		5.735	649.8	1106.6
trans	22.72	55.116	1246.5	1543.7
		60.851	3281.3	3658.0
HNOH ($^2A''$)		5.790	424.7	1103.8
cis	28.90	55.432	1313.9	1483.6
		61.221	3219.2	3624.7
H_2NO ($^2A''$)		6.559	987.9	1198.2
	51.60	60.955	1239.4	1593.6
		63.417	3241.0	3320.4
$H_2NO \rightarrow HNOH$		6.567	−2429.5	883.6
	67.08	56.218	1098.0	1377.9
		58.278	2242.2	3239.7
$H_2NO \rightarrow HNO + H$		14.286	−323.4	250.0
	81.04	54.605	432.9	1143.1
		63.846	1430.7	3099.7
$H_2NO \rightarrow H_2 + NO$		8.829	−2062.1	1046.0
	83.30	49.948	1077.7	1361.0
		55.964	1373.5	2534.4
$HNOH \rightarrow HNO + H$		10.361	−928.1	367.2
cis	86.12	54.148	540.2	1095.2
		50.015	1445.1	3141.4
$HNO + H \rightarrow H_2 + NO$		15.831	−2293.2	317.4
	76.70	51.286	556.6	1052.1
		67.117	1287.4	1431.0

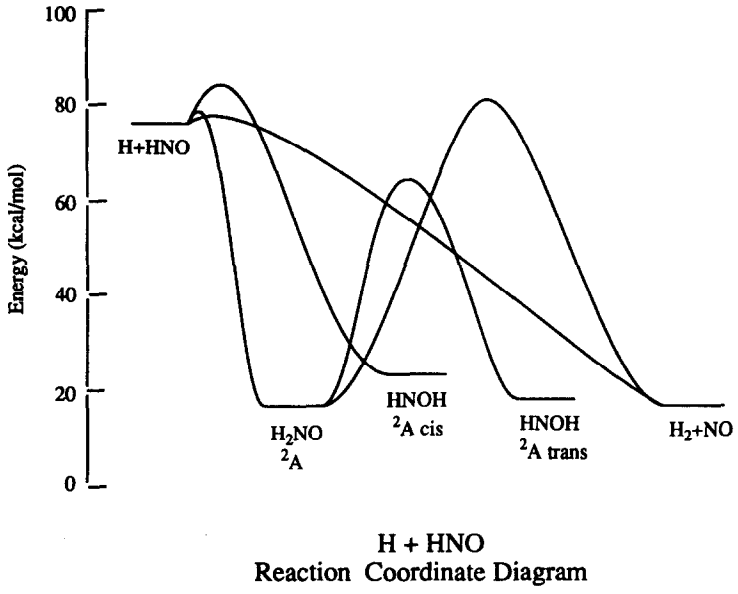

Fig. 19. The energy diagram for the $H + HNO \rightarrow H_2 + NO$ reaction based on the result of BAC-MP4 calculations (this work).

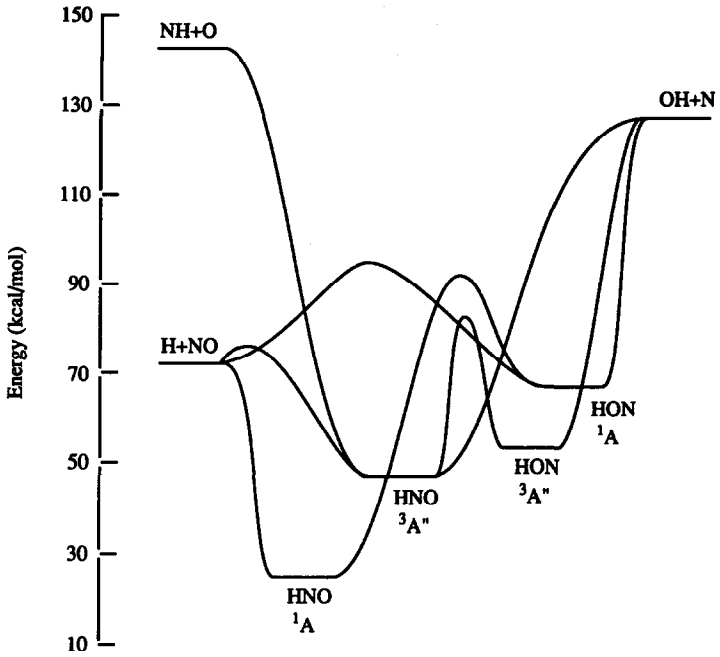

Fig. 20. The energy diagram for the H + NO → N + OH reaction according to the result of BAC-MP4 calculations (this work).

from the fast unimolecular decomposition reaction, HNO + M → H + NO + M.

For the forward process, the most recent measurement of Natarajan and Roth[52] by H-atom resonance absorption spectrometry provides the first direct determination of the rate constant: $k_{16} = 8.5 \times 10^{13} \exp(-27{,}500/T)$ cm^3 mol^{-1} s^{-1}. This result, shown in Fig. 13(a), agrees closely with those obtained from kinetic modeling by Ando and Asaba.[13] The theoretical result of Soto and Page[53] for the reverse abstraction reaction, converted into the forward rate is also fully compatible with the experimental data.

The detailed mechanism and energetics of the H_2 + NO = H + HNO system are summarized in Table 6 and schematically presented in Fig. 19; the figure includes not only the abstraction reaction but also the additional process via the H_2NO radical intermediate: H + HNO $\rightleftharpoons$ $H_2NO \rightarrow H_2$ + NO, computed by the BAC-MP4 method. This process is, however, less important than the direct abstraction reaction because of the tight transition process involved in the molecular elimination process producing H_2 + NO. For the abstraction, Soto and Page's result obtained from a more comprehensive calculation is close to that predicted by the BAC-MP4 method. Both calculations predict the presence of a small reaction barrier for the process (< 1 kcal/mol). In view of the good agreement between the calculated and kinetically modeled H_2 + NO rates, the following expressions, based on Soto and Page's result, are recommended for the forward and the reverse processes over the temperature range 200–3000 K:

$$k_{16} = 6.29 \times 10^{16} T^{-0.89} \exp(-2\,8{,}000/\mathrm{T})\ \mathrm{cm^3\ mol^{-1}\ s^{-1}}.$$

$$k_{-16} = 4.46 \times 10^{11}\ T^{0.72} \exp(-3\,30/\mathrm{T})\ \mathrm{cm^3\ mol^{-1}\ s^{-1}}.$$

5.5. *The H + NO = N + OH Reaction*

The overall rate of NO reduction by H_2 above 1500 K is dominated by the H + NO → N + OH reaction, which provides the major source of O atoms by the rapid, exothermic process, N + NO → N_2 + O. Thus, the H + NO → N + OH reaction is equivalent to the important chain-initiating H + O_2 reaction in the H_2–O_2 system.

Since the production of N + OH from the H + NO reaction is endothermic ($\Delta H° = +48.5$ kcal mol^{-1}), the reaction is controlled by the rate of crossing over the N–OH‡ transition state, rather than by the formation of the HNO and HON intermediates as shown in Fig. 20. Because H and NO are doublet in their ground electronic states, both singlet and triplet HNO and HON may be involved in the reaction as indicated in the figure, which was constructed with the thermochemical data for the intermediates and the transition states computed by the BAC-MP4 method. Their molecular parameters are summarized in Table 7. Also included in the table and the figure are the reaction path for the production of NH + O from N + OH involving the quintet curve which correlates the N(^{4}S) + OH($^2\Pi$) reactants with the NH ($^3\Sigma$) + O (^3P_j) products.

Table 7. Molecular parameters of the H + NO system based on the BAC/MP4 method

Species	$\Delta H^{\circ}_{f,o}$/kcal mol^{-1}	I_A, I_B, I_C/amu	ν_i/cm^{-1}
HNO (^{1}A)	24.06	3.034	1550.1
		40.312	1759.8
		43.346	2986.6
HON (^{1}A)	61.76	2.611	1351.5
		44.675	1453.7
		47.286	3402.1
HNO (^{3}A)	46.21	2.805	886.8
		44.371	1349.6
		47.176	3224.0
HON (^{3}A)	50.72	2.664	1147.1
		49.313	1225.1
		51.976	3580.3
HNO → NOH (^{3}A)	86.07	3.220	−2660.7
		43.182	1364.2
		46.402	2721.4
HNO (^{3}A) → H + NO	77.34	6.748	−1171.3
		41.374	500.6
		48.123	1735.8
HNO (^{3}A) → HON	81.21	3.615	−2262.3
		44.981	1251.0
		48.595	2259.6
HON (^{3}A) → NO + H	89.30	5.926	−1424.3
		43.892	668.3
		49.818	1314.7
NH + O → N + OH	148.06	0.000	−3101.0
		164.926	649.8
		164.926	523.6
			620.3

The validity and reliability of the H$^+$ NO → N + OH reaction rate constant recommended by Hanson and Salimian[1] can be checked with the reverse N + OH → H + NO rate constant, which has been determined by several groups.[55–58] The results of both forward and reverse reactions are summarized in Fig. 13. Employing Hanson and Salimian's recommended value, $k_{54} = 1.70 \times 10^{14} \exp(-24{,}560/T)$ cm^3 mol^{-1} s^{-1}, and the equilibrium constant evaluated from JANAF thermochemical data, we obtain $k_{-54} = 5.10 \times 10^{13} \exp(-130/T)$ cm^3 mol^{-1} s^{-1}. The equation gives $k_{-54} = 3.3 \times 10^{13}$ cm^3 mol^{-1} s^{-1} at 300 K, agreeing closely with the value 3.1×10^{13} cm^3 mol^{-1} s^{-1} computed at the same temperature with the equation recommended by Atkinson *et al.*,[58] $k_{-54} = 2.3 \times 10^{13} \exp(+86/T)$ cm^3 mol^{-1} s^{-1}, based on the results summarized in Fig. 13 (b). The excellent consistency is also graphically illustrated in the figure. The rate constant expression, $k_{-54} = 5.1 \times 10^{13} \exp(-130/T)$ cm^3 mol^{-1} s^{-1} is, therefore, valid for the very broad temperature range 250–4200 K.

6. CONCLUDING REMARKS

The kinetics and mechanisms for the reduction of NO by H_2 initiated photolytically and thermally under well defined temperature and pressure conditions have been modeled with the aid of *ab initio* quantum-chemical and statistical-theory calculations. The results of our modeling, covering a broad temperature range of 80–4500 K, under varying reactant concentration conditions, allow us to identify several key elementary processes.

Some of these processes have been mechanistically elucidated by us for the first time in this and earlier studies. All the processes involve HNO as a reactant(s) or as a reaction intermediate. They dominate the reduction process in different temperature and NO concentration regimes as indicated below:

- $T < 900$ K (photo-induced reaction)
  NO-lean conditions:
  HNO + HNO → *cis*/*trans*-$(HNO)_2$
  NO-rich conditions:
  HNO + 2NO → HN_2O + NO_2
- 900 K < T < 1500 K
  H_2 + NO → H + HNO (reaction initiator)
  HNO + NO → N_2O + OH
  (chain propagator)

$H_2 + NO \rightarrow H + HNO$
(reaction initiator)
$H + NO \rightarrow N + OH$
(chain propagator)

The $H_2 + NO \rightarrow H + HNO$ reaction given above is important only in terms of the reaction initiation; it does not dominate the measured rates of NO reduction throughout the entire range of the thermal reaction above 900 K. The initiation reaction, however, can be effectively measured with the H-atom resonance absorption method in the early stage of the reaction, according to the result of our sensitivity analysis.

The rate constants for these key reactions are recommended for their specific, operative temperature ranges. Long extrapolation of the rate constants for the low-temperature ($T < 900$ K) processes to far beyond the recommended operative range should be avoided, particularly for the $HNO + HNO \rightarrow cis/trans\text{-}(HNO)_2$ recombination process because of the expected strong pressure effect at higher temperatures.

Acknowledgements—The authors gratefully acknowledge the support of this work by the Office of Naval Research to Emory University (Contract No. N00014-89-J-1494) and to Sandia National Laboratories (Contract No. N00014-90-F-0078), under the direction of Dr R. S. Miller.

REFERENCES

1. Hanson, R. K. and Salimian, S., *Survey of rate constants in the NHO system combustion chemistry*, W. C. Garginer, Jr, Ed., Springer, NY (1984).
2. Tsang, W. and Herron, J. T., *J. Phys. Chem. Ref. Data* **20**, 609 (1991).
3. Hinshelwood, C. N. and Green, T. E., *J. Chem. Soc.* 730 (1926).
4. Hinshelwood, C. N. and Mitchell, J. W., *J. Chem. Soc.* 378 (1936).
5. Kaufman, F. and Decker, L. J., *Symp. Int. Combust. Proc.* **8**, 139 (1959).
6. Diau, E. W. G., Halbgewachs, M. J., Smith, A. and Lin, M. C., in preparation.
7. Graven, W. M., *J. Am. Chem. Soc.*, **79**, 3657 (1957).
8. McCullough, R. W., Kruger, C. H. and Hanson, R. K. *Combust. Sci. Technol.* **15**, 213 (1977).
9. Koshi, M., Ando, H., Oya, M. and Asaba, T., *Symp. Int. Combust. Proc.* **15**, 909 (1975).
10. Flower, W. L., Hanson, R. K. and Kruger, C. H., *Symp. Int. Combust. Proc.* **15**, 823 (1975).
11. Bradley, J. N. and Craggs, P., *Symp. Int. Combust. Proc.* **15**, 833 (1975).
12. Duxbury, J. and Pratt, N. H., *Symp. Int. Combust. Proc.* **15**, 843 (1975).
13. Ando, H. and Asaba, T., *Int. J. Chem. Kin.* **8**, 259 (1976).
14. Flower, W. L., Hanson, R. K. and Kruger, C. H., *Combust. Sci. Technol.* **15**, 115 (1977).
15. Lin, M. C., He, Y. and Melius, C. F., *Int. J. Chem. Kin.* **24**, 489 (1992).
16. Melius, C. F. and Binkeley, J. S., *Symp. Int. Combust. Proc.* **20**, 575 (1984).
17. Melius, C. F. In *Chemistry and Physics of Energetic Materials*, S. N. Bulusu, Ed., p. 21, Kluwer Academic Publishers, Dordrecht, (1990).
18 Ho, P. and Melius, C. F., *J. Phys. Chem.* **94**, 5120 (1990).
19. Lin, C. Y., Wang, H. T., Lin, M. C. and Melius, C. F., *Int. J. Chem. Kin.* **22**, 455 (1990).
20. Wang, N. S., Yang, D. L., Lin, M. C. and Melius, C. F., *Int. J. Chem. Kin.* **23**, 151 (1991).
21. Aldridge, K. H., Liu, X., Lin, M. C. and Melius, C. F., *Int. J. Chem. Kin.* **23**, 947 (1991).
22. He, Y., Liu, X., Lin, M. C. and Melius, C. F., *Int. J. Chem. Kin.* **23**, 1129 (1991).
23. Yang, D. L., Yu, T., Lin, M. C. and Melius, C. F., *J. Chem. Phys.* **97**, 922 (1992).
24. Lin, M. C, He, Y. and Melius, C. F., *Int. J. Chem. Kin.* **24**, 1103 (1992).
25. Lin, M. C., He, Y. and Melius, C. F., *J. Phys. Chem.* **97**, 9124 (1993).
26. He, Y., Lin, M. C., Wu, C. H. and Melius, C. F., *Symp. Int. Combust. Proc.* **24**, 711 (1992).
27. Perry, R. A. and Siebers, D. L., *Nature* **324**, 657 (1986).
28. Callear, A. B. and Carr, R. W., *J. Chem. Soc. Faraday Trans.* **71**, 1605 (1975).
29. Cheskis, S. G., Nadtochenko, V. A. and Sarkisov, O. M., *Int. J. Chem. Kin.* **13**, 1041 (1981).
30 He, Y., Sanders, W. A. and Lin, M. C., *J. Phys. Chem.* **92**, 5074 (1988).
31. He, Y. and Lin, M. C., *Int. J. Chem. Kin.* **24**, 743 (1992).
32. Wilde, K. A., *Combust. Flame* **13**, 193 (1969).
33. Lutz, A. E., Kee, R. J. and Miller, J. A., *SENKIN: A Fortran Program for Predicting Homogeneous Gas-Phase Chemical Kinetics with Sensitivity Analysis*, Sandia National Laboratories, Report No. SAND87-8248 (1988).
34. Laidler, K. J., *Chemical Kinetics*, 3rd. ed., Harper and Row (1987).
35. Forst, W., *Theory of Unimolecular Reactions*, Academic, NY (1973).
36. Strausz, O. P. and Gunning, H. E., *Can. J. Chem.* **41**, 1207 (1963).
37. Strausz, O. P. and Gunning, H. E., *Trans. Faraday Soc.* **60**, 347 (1964).
38. Holmes, J. L. and Sundaram, E. V., *Trans. Faraday Soc.* **62**, 910 (1966).
39. Holmes, J. L. and Sundaram, E. V., *Trans. Faraday Soc.* **62**, 1822 (1966).
40. Heicklen, H. and Cohen, N., *Adv. Photochem.* **5**, 157 (1968).
41. Kohout, F. C. and Lampe, F. W., *J. Chem. Phys.* **46**, 4075 (1967).
42. Baulch, D. L., Drysdale, D. D. and Horne, D. G., *Evaluated Kinetic Data for High Temperature Reactions. Vol. 2, Homogeneous Gas Phase Reactions of the H_2–N_2–O_2 Systems*, Butterworth, London (1973).
43. Phillips, L., *J. Chem. Soc.* 3082 (1961).
44. Batt, L., Milne, R. T. and McCullock, R. D., *Int. J. Chem. Kin.* **9**, 549 (1977).
45. Batt, L. and Milne, R. T., *Int. J. Chem. Kin.* **9**, 567 (1977).
46 O'Neal, H. E. and Benson, S. W., *Kinetic Data on Gas Phase Unimolecular Reactions*, NSRDS-NBS 21, Washington, D.C., 1970.
47. Page, M., Lin, M. C., He, Y. and Choudhury, T. K., *J. Phys. Chem.* **93**, 4404 (1989).
48. Choudury, T. K., He, Y., Sanders, W. A. and Lin, M. C., *J. Phys. Chem.* **94**, 2394 (1990).
49. Christie, M. I., Frost, J. S. and Voisey, M. A., *Trans. Faraday Soc.* **61**, 674 (1965).
50. Christie, M. I., *Proc. Roy. Soc.* **A249**, 248 (1959).
51. Kee, R. J., Rupley, F. M. and Miller, J. A. *CHEMKIN-II: A Fortran Chemical Kinetics Package for the Analysis of Gas-Phase Chemical Kinetics*, Sandia National Laboratories, Report No. SAND87-8248, 1988.

52. Natarajan, K. and Roth, P., *19th Int. Symp. on Shock Waves*, Session PCP1, Marseille, France, July 26–30, 1993.
53. Soto, M. R. and Page, M., *J. Chem. Phys.* **97**, 7287 (1992).
54. Chase, M. W., Jr., Davies, C. A., Downley, J. R., Jr, Frurip, D. J., McDonald, R. A. and Syverud, A. N., *J. Phys. Chem. Ref. Data, Suppl. No. 1*, **14**, 1 (1985).
55. Howard, M. J. and Smith, I. W. M., *Chem. Phys. Lett.* **69**, 40 (1980).
56. Howard, M. J. and Smith, I. W. M., *J. Chem. Soc., Faraday Trans. 2*, **77**, 997 (1981).
57. Brune, W. H., Schwab, J. J. and Anderson, J. G., *J. Chem. Phys.* **87**, 4503 (1983).
58. Atkinson, R., Baulch, D. L., Cox, R. A., Hampson, R. F., Jr, Kerr, J. A. and Troe, J. *J. Phys. Chem. Ref. Data*, **18**, 881 (1989).
59. Smith, M. Y., *Combust. Flame* **18**, 293 (1972).
60. Dodonov, A. F., Zelenove, V. V., Tal'roze, V. L., *Dokl. Phys. Chem.* **252**, 642 (1980).
61. Dodonov, A. F., Zelenove, V. V., Strunin, V. P., Tal-'roze, V. L., *Kinet. Catal.* **22**, 689 (1981).
62. Washida, N., Akimoto, H. and Okuda, M., *Phys. Chem.* **82**, 2293 (1978).
63. Clyne, M. A. A. and Thrush, B. A., *Discuss. Faraday Soc.* **33**, 139 (1962).
64. Lambert, R. M., *Chem. Commun.* 850 (1966).
65. Bulewicz, E. M. and Sugden, T. M., *Proc. R. Soc. Lond.* **277**, 143 (1964).
66. Halstead, C. J. and Jenkins, D. R., *Chem. Phys. Lett.* **2**, 281 (1968).
67. He, Y., Liu, X., Lin, M. C. and Melius, C. F., *Int. J. Chem. Kin.* **25**, 845 (1993).
68. Wu, C. H., He, Y. and Lin, M. C., *Proc. 1st Int. Conf. on Combustion Technol. for a Clean Environ., Reaction Fundamentals II*, Vilamoura, Portugal, 3–6 Sept., pp. 19–25 (1991).
69. Mebel, A. M., Morokuma, K., Lin, M. C. and Melius, C. F., *J. Phys. Chem.*, submitted.